CP violation in SM diboson measurement

Qiang Li (Peking University)

2023/08/26 USTC

FIND论坛系列学术研讨会:

FIND CP violation at electroweak scale and beyond

Seattle Snowmass Summer Meeting 2022

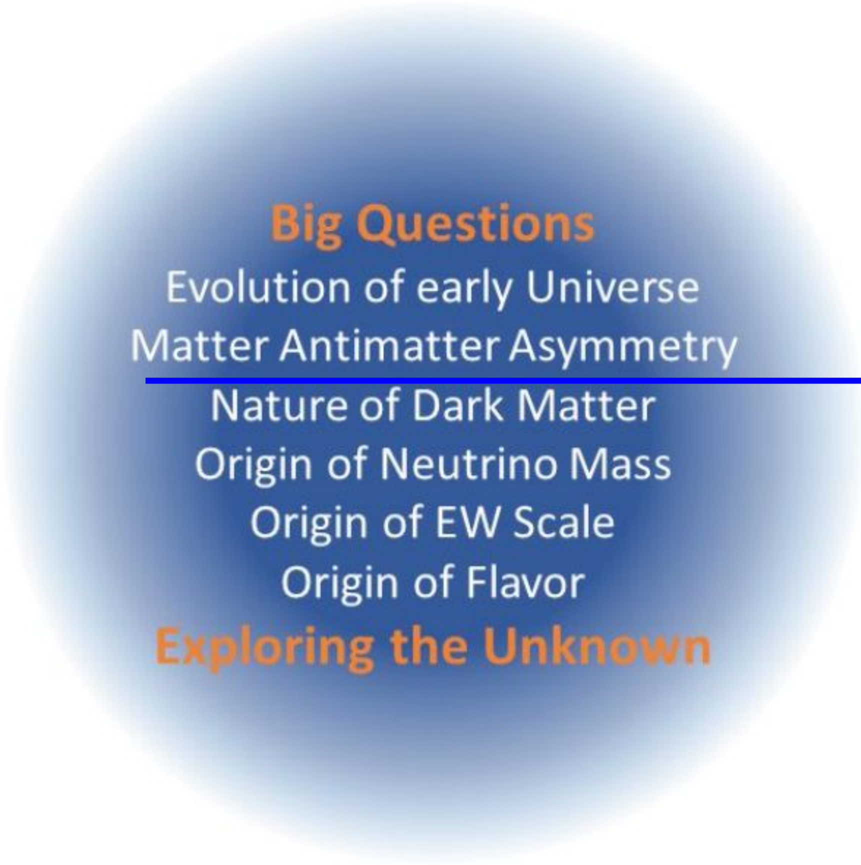

高能量前沿重大问题：

早期宇宙演化、

正反物质不对称性、

暗物质性质、

中微子质量起源、

电弱标度起源、

味道起源 等

Seattle Snowmass Summer Meeting 2022

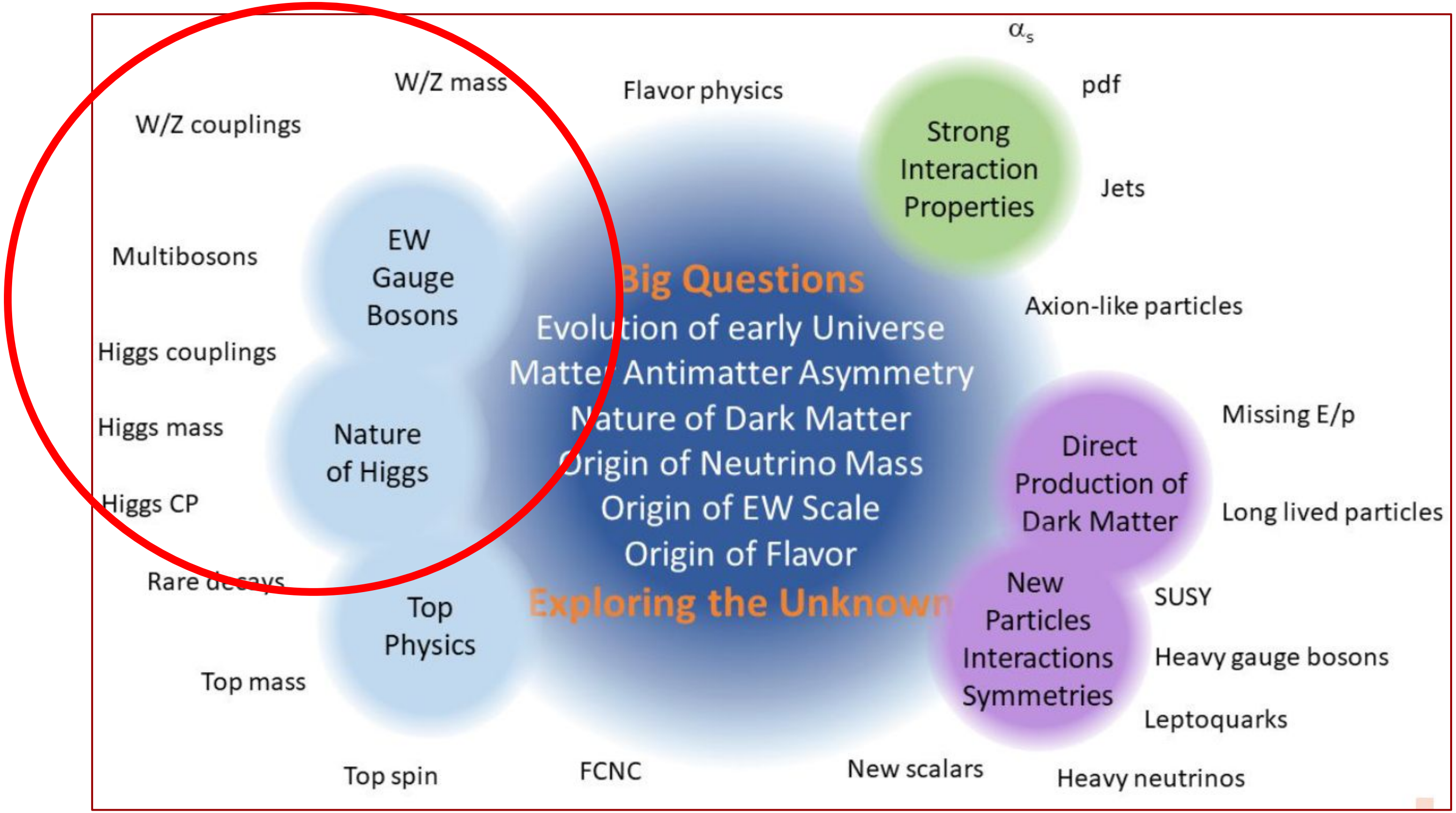

Direct and Indirect Searches for BSM

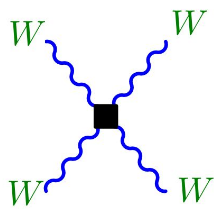

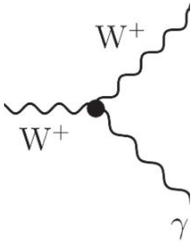

Multiboson as a key tool

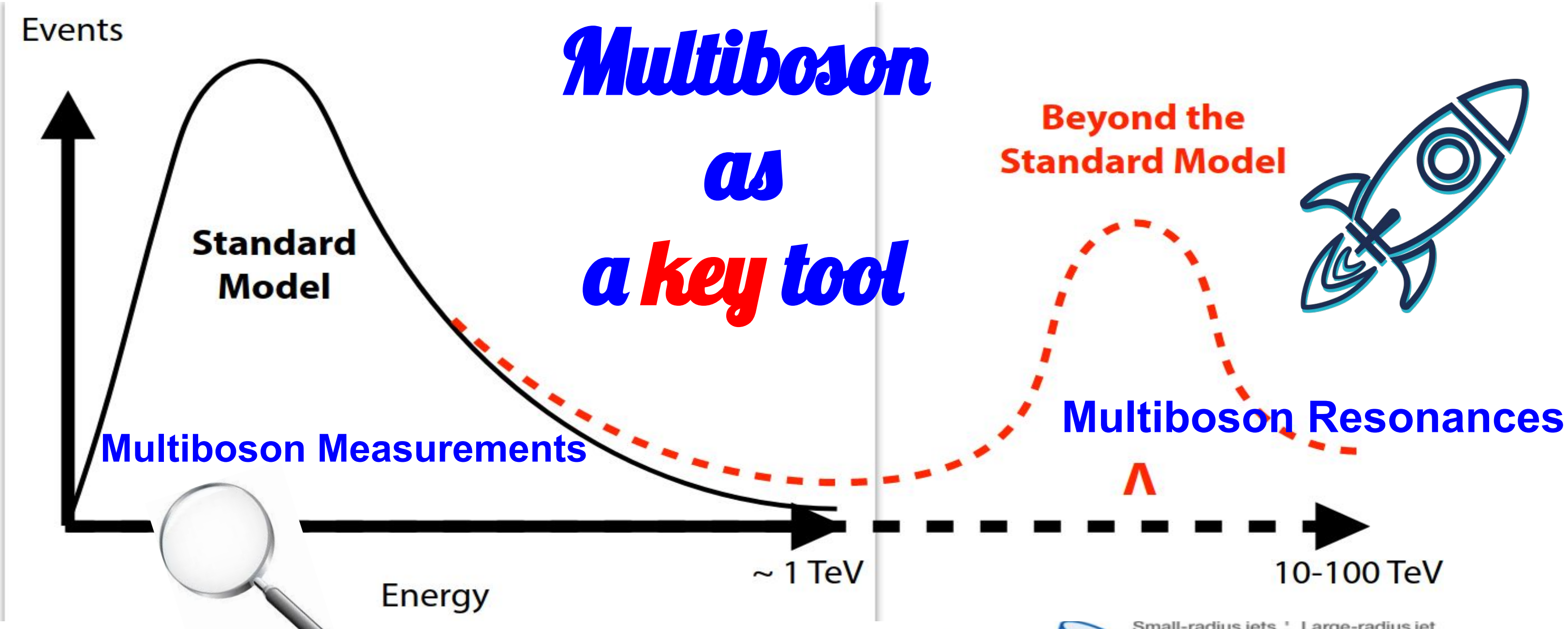

Anomalous couplings, EFT (CP even or odd)

$$L_{\mathrm{EFT}} = L_{\mathrm{SM}} + \sum_i \frac{C_i^{(6)}}{\Lambda^2}\mathcal{O}_i^{(6)} + \sum_i \frac{C_i^{(8)}}{\Lambda^4}\mathcal{O}_i^{(8)} + \ldots$$

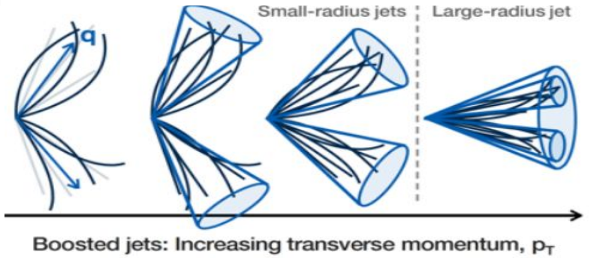

Great Potential to explore unknown

The large boson-boson collider

[Symmetry](#)

High energy.
High multiplicity.
High opportunities?

[Brian Henning](#)

$$|H|^2 \sim (v+h)^2 + \vec{\phi}^2$$

ops that modify HC will induce processes with longitudinal vectors

HC: $|H|^2\,\mathcal{O}_{\rm SM} \supset vh\mathcal{O}_{\rm SM}$

HwH: $|H|^2\,\mathcal{O}_{\rm SM} \supset \vec{\phi}^2\mathcal{O}_{\rm SM}$

Higgs Couplings without the Higgs

		HC	HwH	Growth
κ_t	$\mathcal{O}_{y_t}$	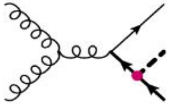	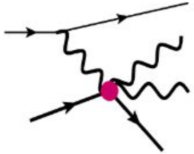	$\sim(E^2/\Lambda^2)$
κ_λ	$\mathcal{O}_6$	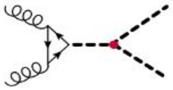	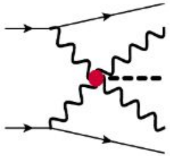	$\sim(vE/\Lambda^2)$
$\kappa_{Z\gamma}$ $\kappa_{\gamma\gamma}$ κ_V	$\mathcal{O}_{WW}$ $\mathcal{O}_{BB}$ $\mathcal{O}_r$	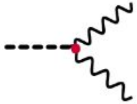	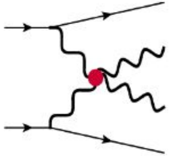	$\sim(E^2/\Lambda^2)$
κ_g	$\mathcal{O}_{gg}$	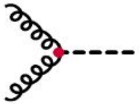	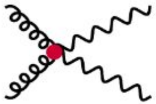	$\sim(E^2/\Lambda^2)$

Rich Results from Multiboson Measurements

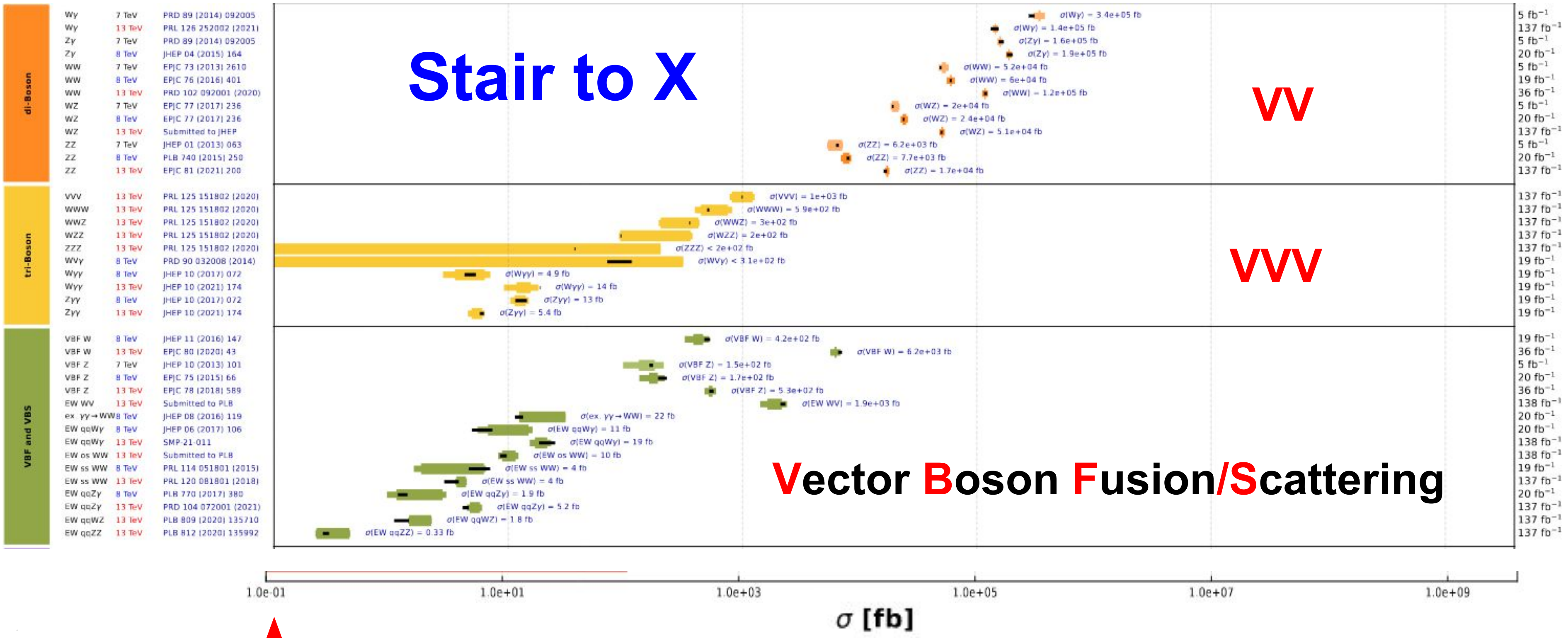

0.1fb

CMS SM Summary Plot 2022/9 (see also ATLAS)

CP Violation in di-boson…

SMEFT (e.g.: Celine Degrande, Julien Toucheque): 10 CP-odd operators integrated in a FeynRules model with massless fermions and UFO package ready to use in MC event generators.

Impose $U(1)^{14}$ symmetry

Hermitian and non-Hermitian operators

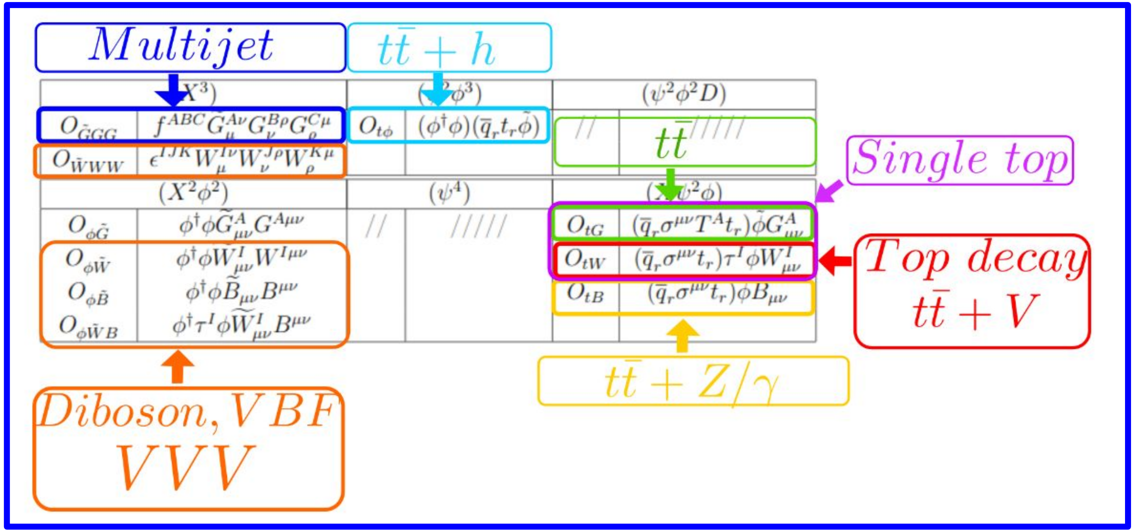

EWDim6/HISZ

$$\delta\mathcal{L}_{AC} = \frac{c_{WWW}\,\mathrm{Tr}[W_{\mu\nu}W^{\nu\rho}W^{\mu}_{\rho}] + c_{W}\left(D_\mu\Phi\right)^\dagger W^{\mu\nu}\left(D_\nu\Phi\right) + c_{b}\left(D_\mu\Phi\right)^\dagger B^{\mu\nu}\left(D_\nu\Phi\right)}{\Lambda^2} + \frac{\tilde{c}_{WWW}\,\mathrm{Tr}[\widetilde{W}_{\mu\nu}W^{\nu\rho}W^{\mu}_{\rho}] + \tilde{c}_{W}\left(D_\mu\Phi\right)^\dagger \widetilde{W}^{\mu\nu}\left(D_\nu\Phi\right)}{\Lambda^2}$$

Different conventions...

SMEFT

Wilson Coefficient	Operator
C_W (C_{WWW})	$\epsilon^{abc}W_\mu^{a\nu}W_\nu^{b\rho}W_\rho^{a\mu}$
C_{HD}	$\lvert H^\dagger(D_\mu\Phi)\rvert^2$
C_{HWB}	$H^\dagger\sigma^a\Phi W^a_{\mu\nu}B^{\mu\nu}$
$C_{Hl}^{(1)}$	$(H^\dagger i\overleftrightarrow{D}_\mu H)(\bar{l}_p\gamma^\mu l_r)$
$C_{Hl}^{(3)}$	$(H^\dagger i\overleftrightarrow{D}_\mu H)(\bar{l}_p\tau^I\gamma^\mu l_r)$
$C_{Hq}^{(1)}$	$(H^\dagger i\overleftrightarrow{D}_\mu H)(\bar{q}_p\gamma^\mu q_r)$
$C_{Hq}^{(3)}$	$(H^\dagger i\overleftrightarrow{D}_\mu H)(\bar{q}_p\tau^I\gamma^\mu q_r)$
C_{Hud}	$i\left(\tilde{H}^\dagger D_\mu H\right)\bar{u}_R\gamma^\mu d_R$
C_{ll}	$(\bar{l}_p\gamma_\mu l_r)(\bar{l}_s\gamma^\mu l_t)$
C_{Hd}	$(H^\dagger i\overleftrightarrow{D}_\mu H)(\bar{d}_p\gamma^\mu d_r)$

Table 1: The various other dim-6 EFT operators.

EWDim6/HISZ

The minimal set of dimension-6 operators explored in CMS in WW and WZ final states are the following:

$$\mathcal{O}_{WWW} = \mathrm{Tr}\,[W_{\mu\nu}W^{\nu\rho}W_\rho^\mu] \tag{1.1}$$
$$\mathcal{O}_W = (D_\mu\Phi)^\dagger W^{\mu\nu}(D_\nu\Phi) \tag{1.2}$$
$$\mathcal{O}_B = (D_\mu\Phi)^\dagger B^{\mu\nu}(D_\nu\Phi) \tag{1.3}$$

which are the three C and P conserving operators. In addition, there are two additional C and P violating operators are:

$$\mathcal{O}_{\tilde{W}WW} = \mathrm{Tr}\,[\tilde{W}_{\mu\nu}W^{\nu\rho}W_\rho^\mu] \tag{1.4}$$
$$\mathcal{O}_{\tilde{W}} = (D_\mu\Phi)^\dagger \tilde{W}^{\mu\nu}(D_\nu\Phi) \tag{1.5}$$

These operators seem to be defined in an *ad-hoc* basis first making their appearance in Ref. [1] and subsequently in Ref. [2].

[1] K. Hagiwara et al. "Low energy effects of new interactions in the electroweak boson sector" Phy. Rev. D Vol 48 No. 5

[2] C. Degrande et al. "Effective Field Theory: A Modern Approach to Anomalous Couplings" arXiv:1205.4231

Ref $\quad \mathcal{O}_{WWW} = \frac{g^3}{4}Q_W\,,$

ATLAS VBF Z

Wilson coefficient	Includes $|\mathcal{M}_{d6}|^2$	95% confidence interval [TeV^{-2}] Expected	Observed	p-value (SM)
c_W/Λ^2	No	$[-0.30,\ 0.30]$	$[-0.19,\ 0.41]$	45.9%
	Yes	$[-0.31,\ 0.29]$	$[-0.19,\ 0.41]$	43.2%
$\tilde{c}_W/\Lambda^2$	No	$[-0.12,\ 0.12]$	$[-0.11,\ 0.14]$	82.0%
	Yes	$[-0.12,\ 0.12]$	$[-0.11,\ 0.14]$	81.8%
c_{HWB}/Λ^2	No	$[-2.45,\ 2.45]$	$[-3.78,\ 1.13]$	29.0%
	Yes	$[-3.11,\ 2.10]$	$[-6.31,\ 1.01]$	25.0%
$\tilde{c}_{HWB}/\Lambda^2$	No	$[-1.06,\ 1.06]$	$[0.23,\ 2.34]$	1.7%
	Yes	$[-1.06,\ 1.06]$	$[0.23,\ 2.35]$	1.6%

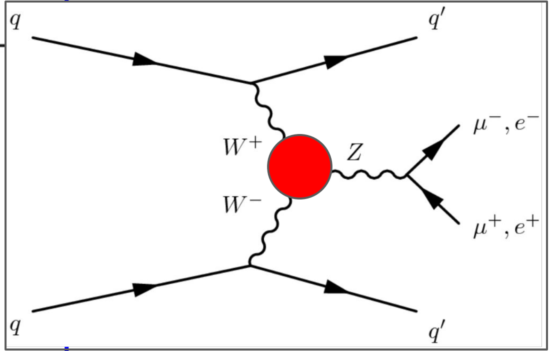

The 95% confidence intervals for the CP-even and CP-odd operators can be translated into the HISZ basis [83–85] and be compared with previous ATLAS and CMS results. The observed and expected 95% confidence intervals for the c_{WWW}/Λ^2 Wilson coefficient are [–2.7, 5.8] TeV^{-2} and [–4.4, 4.1] TeV^{-2}, respectively. The observed and expected 95% confidence intervals for the $\tilde{c}_{WWW}/\Lambda^2$ Wilson coefficient are [–1.6, 2.0] TeV^{-2} and [–1.7, 1.7] TeV^{-2} respec-

$$\mathcal{O}_{WWW} = \frac{g^3}{4} Q_W\,,$$

CWWW:
EWDim6/SMEFT~14.2

Current LHC related limits

1 ATLAS VBF W
2 ATLAS VBF Z

Operators	$\sigma(pp \to Wjj)$ [1]	$\Delta\phi_{jj}(pp \to Zjj)$[2]	EDMs[3]
$\mathcal{O}_{\widetilde{W}WW}$	[-14, 14] (expected) [-11, 11] (measured)	[-0.12, 0.12] (expected) [-0.11, 0.14] (measured)	$\leq 1.74\ 10^{-4}$
$\mathcal{O}_{\phi\widetilde{W}B}$	// //	[-1.06, 1.06] (expected) [-0.23, 2.34] (measured)	$\leq 5.57\ 10^{-6}$

Table: Collection of the constraints on the two dimension-six operators with $\Lambda = 1$TeV at 95% CL.

3: CMS WZ

Parameter	95% CI, exp. (TeV^{-2})	95% CI, obs. (TeV^{-2})	Best fit, obs. (TeV^{-2})
c_{W}/Λ^2	$[-2.0, 1.3]$	$[-2.5, 0.3]$	-1.3
c_{WWW}/Λ^2	$[-1.3, 1.3]$	$[-1.0, 1.2]$	0.1
c_{b}/Λ^2	$[-86, 125]$	$[-43, 113]$	44
$\tilde{c}_{WWW}/\Lambda^2$	$[-0.76, 0.65]$	$[-0.62, 0.53]$	-0.03
$\tilde{c}_{W}/\Lambda^2$	$[-46, 46]$	$[-32, 32]$	0

Current SM related limits

4 ATLAS WW (2016)

Table 6 The expected and observed 95% CL intervals for the anomalous coupling parameters of the EFT model [109]. There is a change in convention relative to Ref. [6] that changes the sign on some of these parameters

Parameter	Observed 95% CL [TeV^{-2}]	Expected 95% CL [TeV^{-2}]
c_{WWW}/Λ^2	[−3.4, 3.3]	[−3.0, 3.0]
c_W/Λ^2	[−7.4, 4.1]	[−6.4, 5.1]
c_B/Λ^2	[−21, 18]	[−18, 17]
$c_{\tilde{W}WW}/\Lambda^2$	[−1.6, 1.6]	[−1.5, 1.5]
$c_{\tilde{W}}/\Lambda^2$	[−76, 76]	[−91, 91]

5 CMS Wγ (2016)

Another one with full Run2 but only CP-even

Coefficient	Exp. lower	Exp. upper	Obs. lower	Obs. upper
c_{WWW}/Λ^2	−0.85	0.87	−0.90	0.91
c_B/Λ^2	−46	45	−40	41
$c_{\overline{W}WW}/\Lambda^2$	−0.43	0.43	−0.45	0.45
$c_{\overline{W}}/\Lambda^2$	−23	22	−20	20

6 CMS ZZ (2016)
7 ATLAS ZZ (Full Run2)

aNTGC

shell Z bosons. These are described by two CP-violating (f_4^V) and two CP-conserving (f_5^V) parameters, where V = Z or γ.

$$-0.0012 < f_4^Z < 0.0010, \quad -0.0010 < f_5^Z < 0.0013,$$
$$-0.0012 < f_4^\gamma < 0.0013, \quad -0.0012 < f_5^\gamma < 0.0013.$$

aNTGC parameter	Interference only		Full	
	Expected	Observed	Expected	Observed
f_Z^4	[−0.16, 0.16]	[−0.12, 0.20]	[−0.013, 0.012]	[−0.012, 0.012]
f_γ^4	[−0.30, 0.30]	[−0.34, 0.28]	[−0.015, 0.015]	[−0.015, 0.015]

interference, BSM, asymmetry, polarization, Optimized observables…

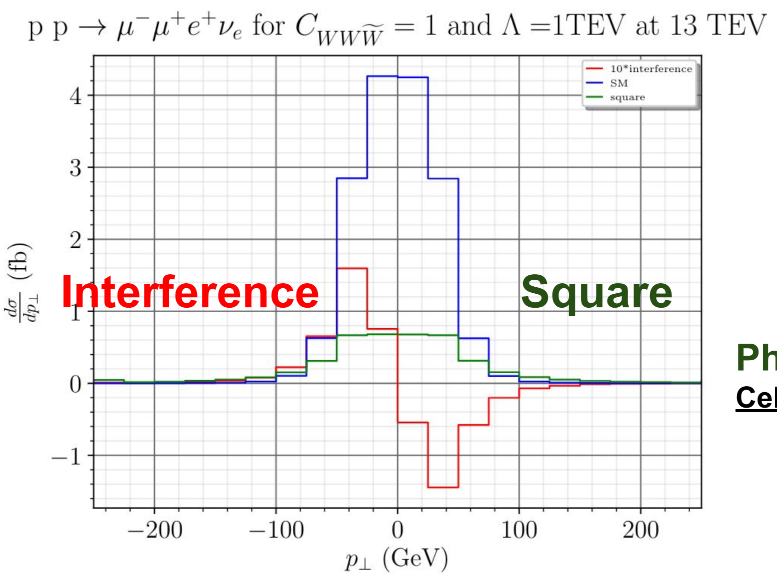

Triple product

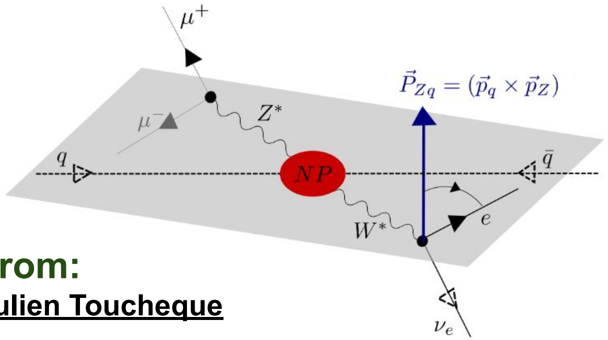

Pheno studies from:

Celine Degrande, Julien Toucheque

- Definition :

$$p_\perp(p_e, p_q) = \vec{p}_e . (\vec{p}_Z \times \vec{p}_q)$$

Those squared amplitudes are CP-even and do contribute to CP-even observables but are more suppressed in $1/\Lambda$. Therefore, analyzing CP-odd operators with the total cross-section is expected to lead to less stringent constraints on their Wilson coefficients but the main drawback is that they do not test whether CP is actually broken. In general, conventional CP-even observables are not suited to efficiently probe CP violating effects since they present no or small variations from expected SM simulations by relying on Λ^{-4}-suppressed effects [33–35].

However, we are not always sensitive to interference yet!

In current LHC di-boson analyses, CP-odd either ignored, or treated same as CP-even

Many talks from this workshop!

7 ATLAS ZZ (Full Run2)

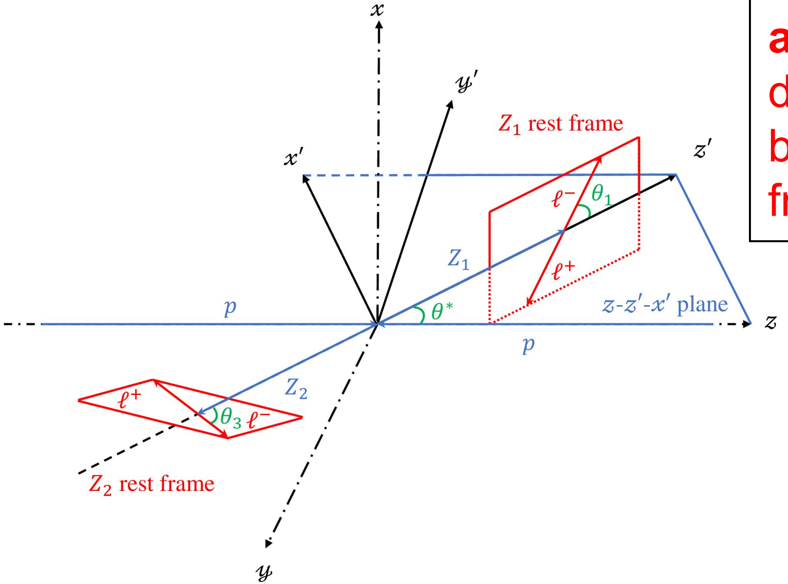

Polar &/or **azimuthal angles** from the diboson rest and boson decay frames

CMS WG (Full Run2)

only for CP-even operator though

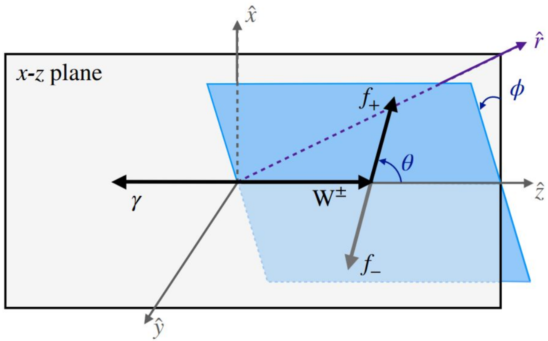

Figure 2: Scheme of the special coordinate system for W$^\pm\gamma$ production, defined by a Lorentz boost to the center-of-mass frame along the direction $\hat{r}$. The z axis is chosen as the W$^\pm$ boson direction in this frame, and y is given by $\hat{z} \times \hat{r}$. The W$^\pm$ boson decay plane is indicated in blue, where the labels f_+ and f_- refer to positive and negative helicity final-state fermions. The angles ϕ and θ are the azimuthal and polar angles of f_+.

To improve the sensitivity, the two CP-sensitive angles $\theta_1(\theta_3)$ and $\phi_1(\phi_3)$ are combined to form an angular observable $T_{yz,1(3)} = \sin\phi_{1(3)} \times \cos\theta_{1(3)}$ which maximises the asymmetry for each Z boson system.

The OO defined for the CP study combines the CP-sensitive polar and azimuthal angles of both Z boson systems, providing additional CP sensitivity from shape differences between the SM and aNTGC predictions. The CP-sensitive polar angles $\theta_1(\theta_3)$ for the $Z_1(Z_2)$ boson are already defined in Section 6.1. The CP-sensitive azimuthal angles ϕ_1 and ϕ_3 are reconstructed in a reference frame that allows a direct measure of the Z boson spin as discussed in Ref. [24, 89] and are illustrated in Figure 2. The CP-sensitive azimuthal angle $\phi_1(\phi_3)$ is the azimuthal angle of the negative lepton in the $Z_1(Z_2)$ rest frame in this new axis system. The differential cross-sections for $\theta_1(\theta_3)$ and $\phi_1(\phi_3)$ are symmetric in the SM but asymmetric in the presence of the two CP-odd aNTGC.

However, we are not always sensitive to interference yet!

Example 1: ATLAS VBF Z+2 Jets

- **Select events consistent with EW Zjj topology**
  - **Opposite charge, same flavor lepton pair**
  - **Dijet system: m_{jj}>1 TeV, $|\Delta y_{jj}|$>2.0**
  - **Z boson centrally produced relative to dijet**
  - **Z boson & dijet required to be approximately balanced in transverse momentum**

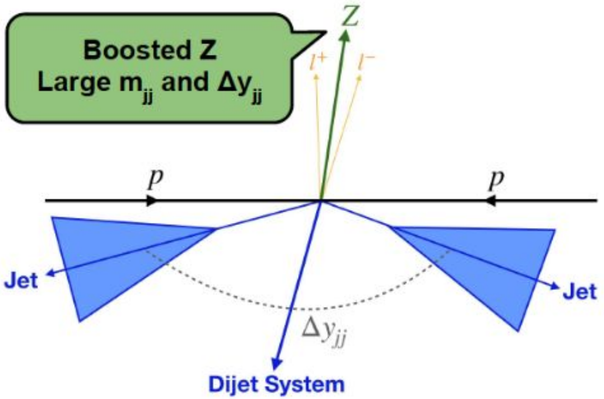

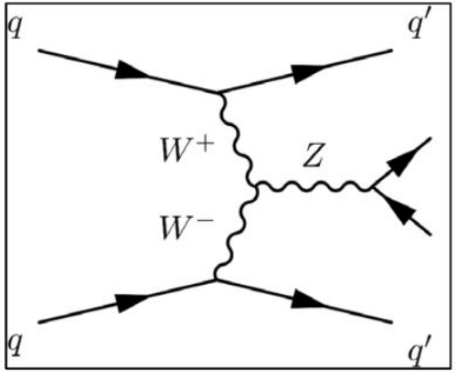

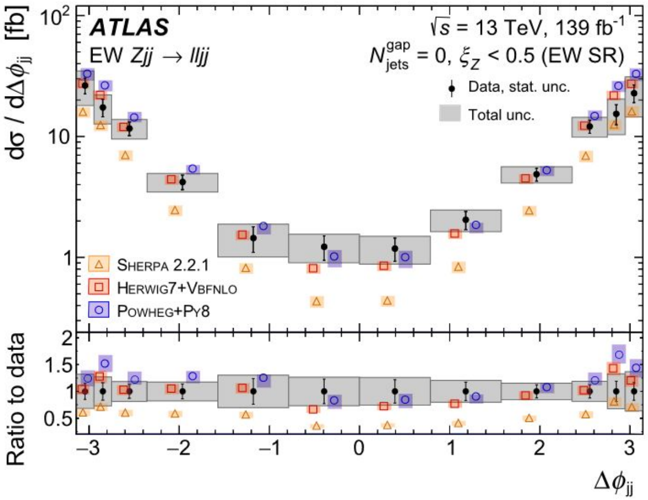

Example 1: ATLAS VBF Z+2 Jets

- **Constraints are placed on dimension-6 operators in Warsaw basis**
  - CP-even: (O_W, O_{HWB})
  - CP-odd: ($\tilde{O}_W$, $\tilde{O}_{HWB}$)
- **$\Delta\phi_{jj}$ is more sensitive to anomalous interactions and therefore used to constrain Wilson coefficients**
  - Constraints on dimension-6 operators, derived with and without pure dimension-6 terms, show much less sensitivity from the pure dimension-6 terms

EFT: $\mathcal{L}_{\text{eff}} = \mathcal{L}_{\text{SM}} + \sum_i \boxed{\frac{c_i}{\Lambda^2}} O_i$

$$|\mathcal{M}|^2 = |\mathcal{M}_{\text{SM}}|^2 + 2\,\text{Re}(\mathcal{M}^*_{\text{SM}}\mathcal{M}_{\text{d6}}) + \boxed{|\mathcal{M}_{\text{d6}}|^2}$$

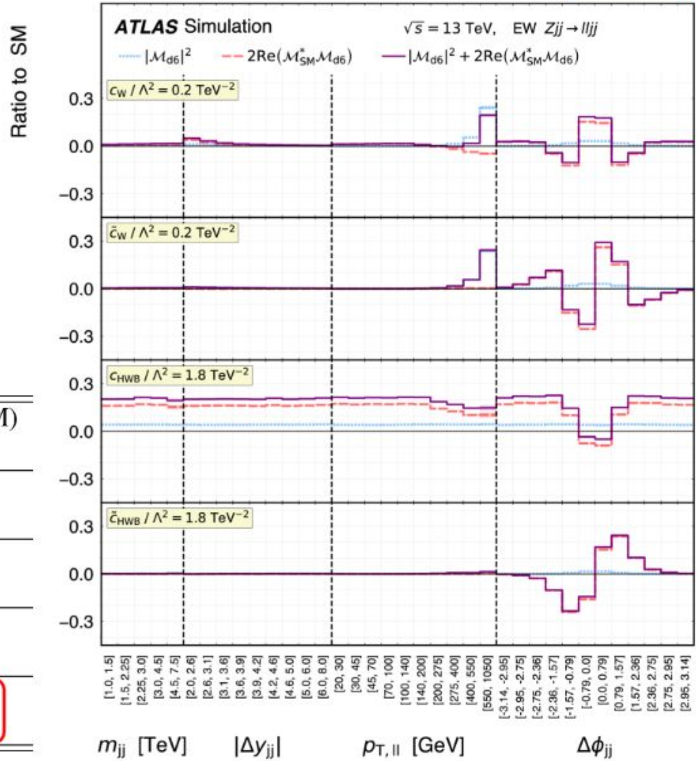

Wilson coefficient	Includes $\|\mathcal{M}_{d6}\|^2$	95% confidence interval [TeV^{-2}] Expected	Observed	p-value (SM)
c_W/Λ^2	no	[−0.30, 0.30]	[−0.19, 0.41]	45.9%
	yes	[−0.31, 0.29]	[−0.19, 0.41]	43.2%
$\tilde{c}_W/\Lambda^2$	no	[−0.12, 0.12]	[−0.11, 0.14]	82.0%
	yes	[−0.12, 0.12]	[−0.11, 0.14]	81.8%
c_{HWB}/Λ^2	no	[−2.45, 2.45]	[−3.78, 1.13]	29.0%
	yes	[−3.11, 2.10]	[−6.31, 1.01]	25.0%
$\tilde{c}_{HWB}/\Lambda^2$	no	[−1.06, 1.06]	[0.23, 2.34]	1.7%
	yes	[−1.06, 1.06]	[0.23, 2.35]	1.6%

Example 2: CMS WZ

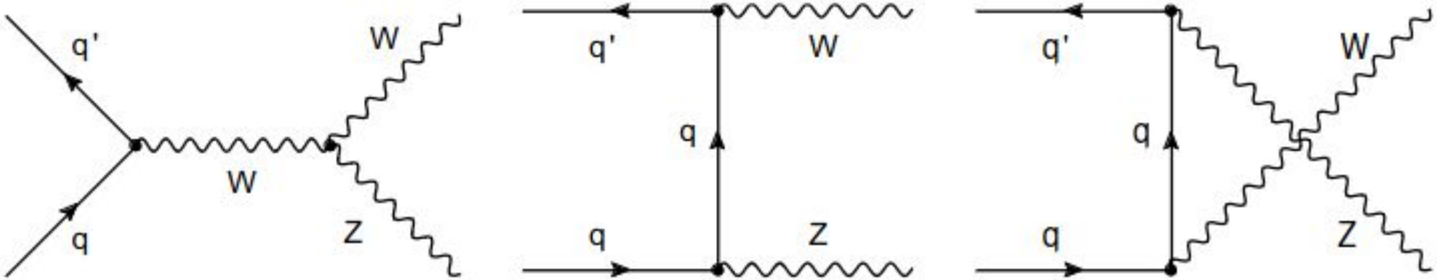

Signal: **powheg box (v2.0) NLO (nominal); MadGraph5_amc@nlo 0+1jet FxFx (alternative)**

Region	N_ℓ	$p_T\{\ell_{Z1}, \ell_{Z2}, \ell_W, \ell_4\}$	N_{OSSF}	$\lvert M(\ell_{Z1}, \ell_{Z2}) - m_Z \rvert$	p_T^{miss}	$N_{b\ tag}$	$\min(M(\ell\ell'))$	$M(\ell_{Z1}, \ell_{Z2}, \ell_W)$
SR	=3	>{25, 10, 25, —} GeV	≥1	<15 GeV	>30 GeV	=0	>4 GeV	>100 GeV
CR-ZZ	=4	>{25, 10, 25, 10} GeV	≥1	<15 GeV	—	=0	>4 GeV	>100 GeV
CR-$t\bar{t}$Z	=3	>{25, 10, 25, —} GeV	≥1	<15 GeV	>30 GeV	>0	>4 GeV	>100 GeV
CR-conv	=3	>{25, 10, 25, —} GeV	≥1	—	≤30 GeV	=0	>4 GeV	<100 GeV

Example 2: CMS WZ

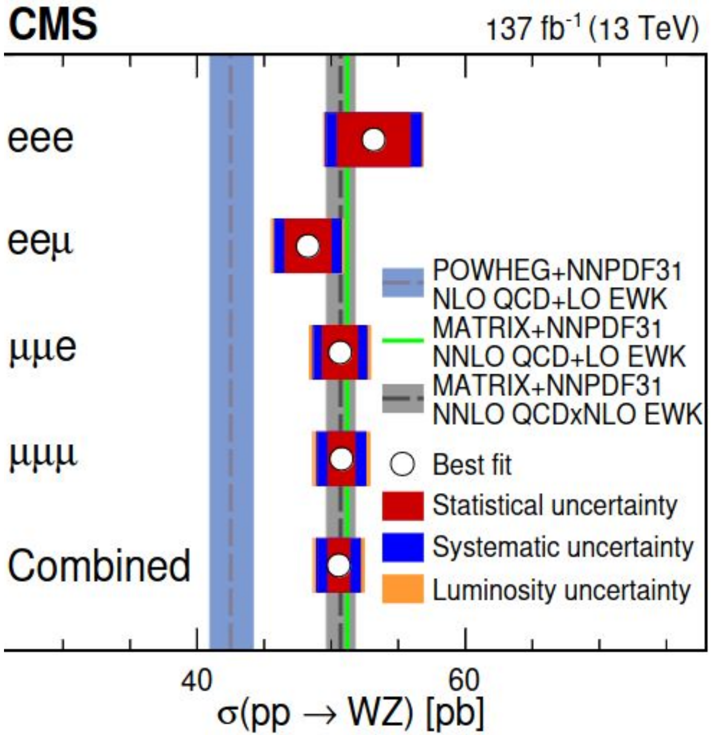

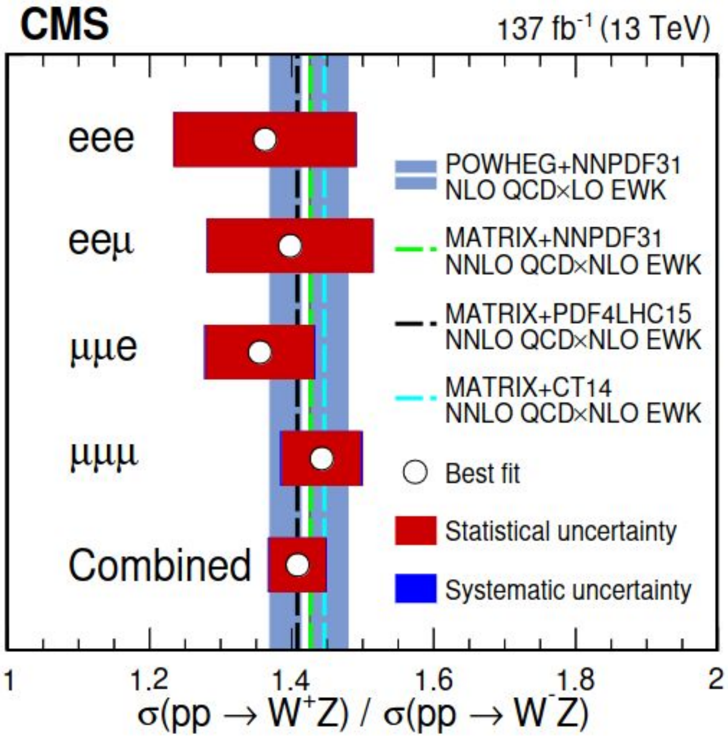

Total cross section measured in a total phase space: 3 light leptons and 60 GeV < mZ < 120 GeV at gen level phase space.

Asymmetry ratio driven by the statistical precision. Effects on PDF also studied using the Bayesian reweighting technique.

Example 2: CMS WZ

⇢ Instead of measuring the spin density matrix, experimental searches have focused on the -related- polarization fractions f_L, f_R, f_0 (left, right, longitudinal).

⇢ The key observable is the "polarization angle" θ_V.

⇢ At LO in EWK, a quadratic dependance of the differential cross-section with respect to $\cos(\theta_V)$ is expected:

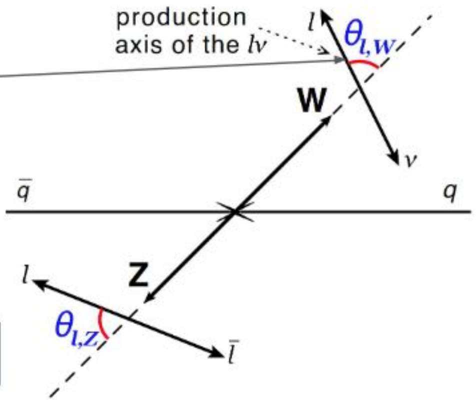

$$\frac{d\sigma}{\sigma d\cos\theta^{W\pm}} = \frac{3}{8}\left[(1 \mp \cos(\theta^{W\pm}))^2 f_L^W + (1 \pm \cos(\theta^{W\pm}))^2 f_R^W + 2\sin^2(\theta^{W\pm}) f_0^W\right]$$

$$\frac{d\sigma}{\sigma d\cos\theta^{Z}} = \frac{3}{8}\left[(1 + \cos^2(\theta^{Z}) + 2c\cos(\theta^{Z})) f_L^Z + (1 + \cos^2(\theta^{Z}) - 2c\cos(\theta^{Z})) f_R^Z + 2\sin^2(\theta^{Z}) f_0^Z\right]$$

⇢ f_0 (longitudinal), and f_L, and f_R (transversal) polarization fractions are the measurable quantities.

⇢ The additional constant "c" for the Z accounts for its couplings to both left and right handed fermions.

⇢ Polarization fractions are frame-dependant for massive particles, so **the frame needs to be fixed**.

https://indico.cern.ch/event/1087104/contributions/4570039/attachments/2348824/4005921/Polarization_LHCEWWG.pdf

Example 2: [CMS WZ](https://indico.cern.ch/event/1087104/contributions/4570039/attachments/2348824/4005921/Polarization_LHCEWWG.pdf)

⇢ The helicity frame defined in **the centre-of mass of the measured gauge boson (W or Z)** is used to perform the measurements of the gauge boson polarization fractions.

⇢ Strictly speaking a different frame for the measurement of each of the bosons, as only singly polarized states are studied.

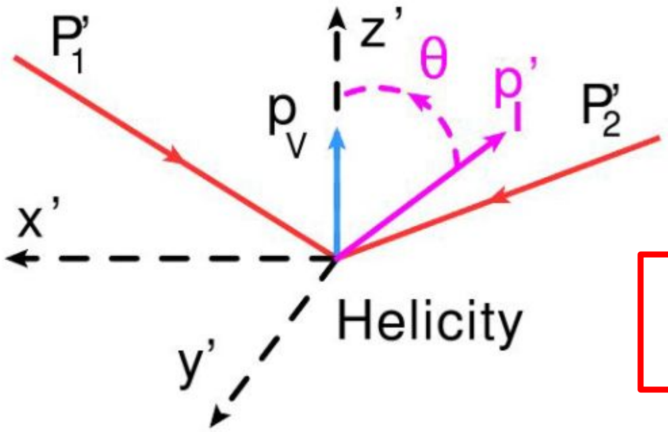

The helicity frame is obtained in two transformations:

1) *Start at the pp frame (O frame), and rotate it so the W (Z) boson momentum goes along the z axis (O' frame).*
2) *The O' frame is then boosted so the W (Z) boson is at rest (O" frame)*

- θ is then the angle between the lepton and the Z axis in the O" frame (helicity frame).

https://indico.cern.ch/event/1087104/contributions/4570039/attachments/2348824/4005921/Polarization_LHCEWWG.pdf

Example 2: CMS WZ: W reconstruction

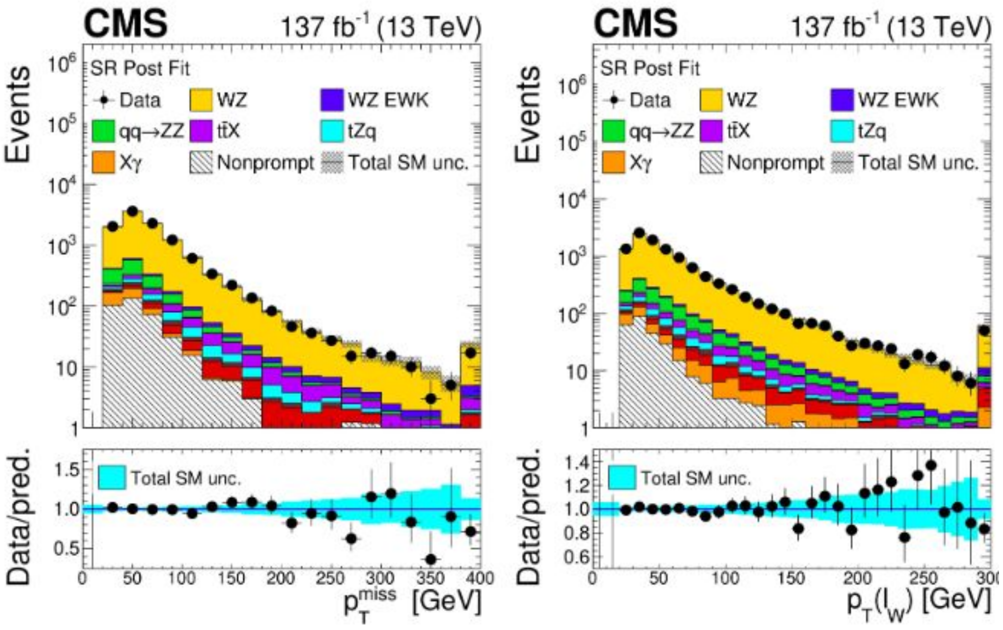

In cases where two real solutions are compatible with the W mass constrain, the one resulting in a lower magnitude of the longitudinal momentum of the neutrino is chosen. If both solutions are complex, their real part is chosen instead.

⇢ W boson is reconstructed from l_W and p_T^{miss}. ⇢ The constraint of $m(l_W, p_T^{miss}) = m_W$ is used to solve for the neutrino's p_Z.

Example 2: CMS WZ

Building polarized templates

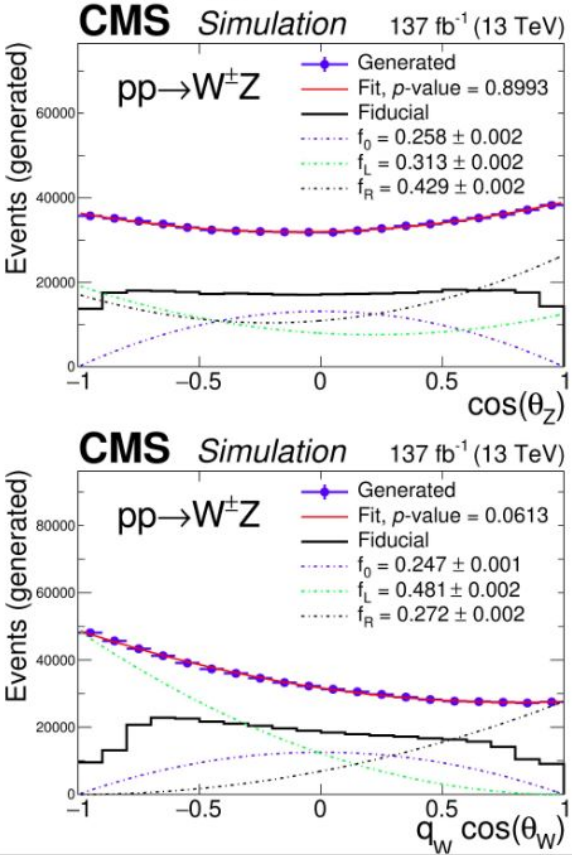

⇢ The procedure is based on the **reweighting of a POWHEG+Pythia sample** based on the generator-level cos(θ_V) distributions to obtain "pure" polarized templates:

⇢ For example, the event weight for the left-handed W templates:

$$\frac{\frac{3}{8}\,(1 \mp \cos\theta_{\ell,W})^2}{\frac{3}{8} f_L^{\text{gen.}} (1 \mp \cos\theta_{\ell,W})^2 + \frac{3}{8} f_R^{\text{gen.}} (1 \pm \cos\theta_{\ell,W})^2 + \frac{3}{4} f_0^{\text{gen.}} \sin^2\theta_{\ell,W}}$$

⇢ The f_0^{gen}, f_L^{gen}, f_R^{gen} quantities can be obtained directly by fitting the cos(θ_V) distribution of the whole sample.

⇢ Fiducial requirements break the quadratic dependance! This fit is not possible at the reco-level.

Example 2: CMS WZ

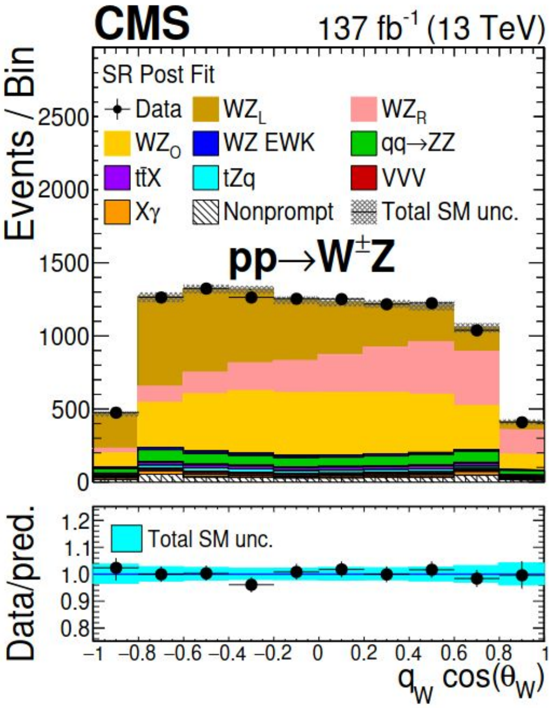

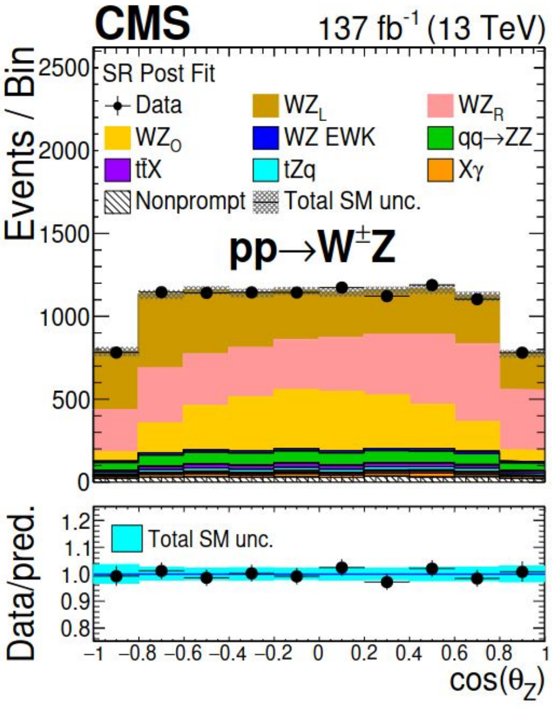

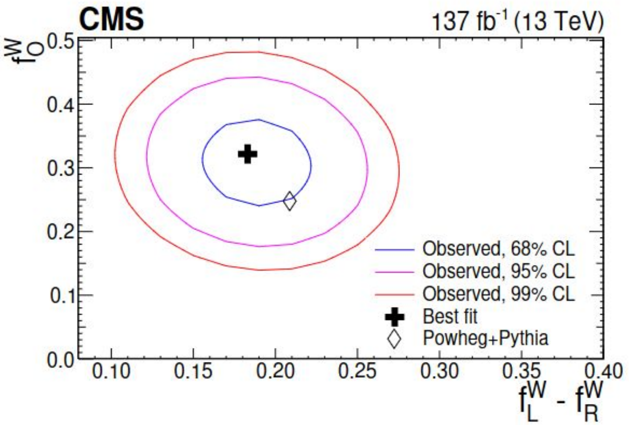

The cos(θ) distributions at the reconstructed are fitted separately for W/Z production. **First observation of single longitudinally polarized W bosons in WZ production! 5.6 σ (4.3σ) obs (exp).**

Example 2: CMS WZ: aGCs

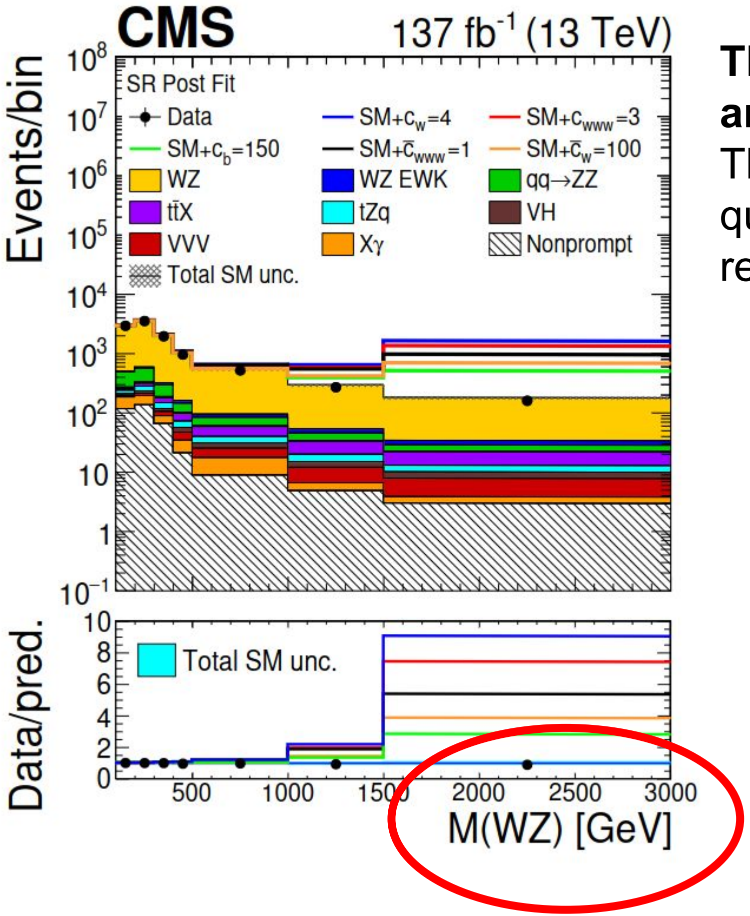

The longitudinal momentum and mass of the neutrino are assumed to be zero in the computation of M(WZ). This choice aims to avoid further correlation of the M(WZ) quantity with the MET variable, which has a worse resolution than the leptonic momenta.

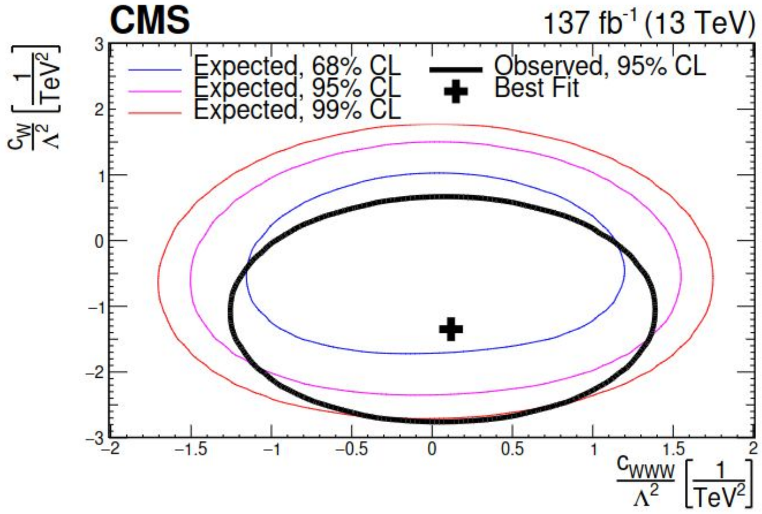

Example 2: CMS WZ:aGCs

Parameter	95% CI, exp. (TeV^{-2})	95% CI, obs. (TeV^{-2})	Best fit, obs. (TeV^{-2})
c_{w}/Λ^2	$[-2.0, 1.3]$	$[-2.5, 0.3]$	-1.3
$c_{\mathrm{www}}/\Lambda^2$	$[-1.3, 1.3]$	$[-1.0, 1.2]$	0.1
c_{b}/Λ^2	$[-86, 125]$	$[-43, 113]$	44
$\widetilde{c}_{\mathrm{www}}/\Lambda^2$	$[-0.76, 0.65]$	$[-0.62, 0.53]$	-0.03
$\widetilde{c}_{\mathrm{w}}/\Lambda^2$	$[-46, 46]$	$[-32, 32]$	0

Both the purely dimension-eight BSM contribution as well as the dimension-six interference term are included

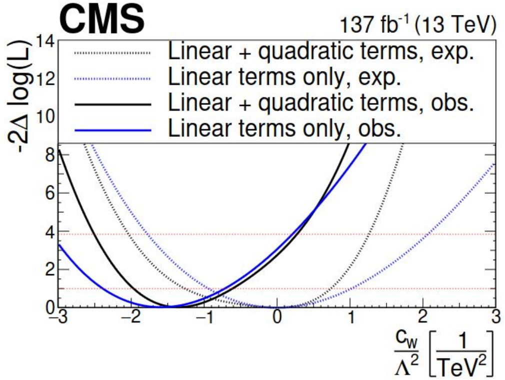

Parameter	95% CI, exp. (TeV^{-2})	95% CI, obs. (TeV^{-2})	Best fit, obs. (TeV^{-2})
c_{w}/Λ^2	$[-1.8, 2.1]$	$[-3.1, 0.3]$	-1.6
$c_{\mathrm{www}}/\Lambda^2$	$[-8.5, 8.5]$	$[-4.2, 14.2]$	5.5
c_{b}/Λ^2	$[-200, 180]$	$[10, 380]$	200
$\widetilde{c}_{\mathrm{www}}/\Lambda^2$	$[-3.3, 4.1]$	$[-4.0, 3.6]$	-0.6
$\widetilde{c}_{\mathrm{w}}/\Lambda^2$	—	—	—

Only the dimension-six interference term is included

Example 2: CMS WZ:aGCs

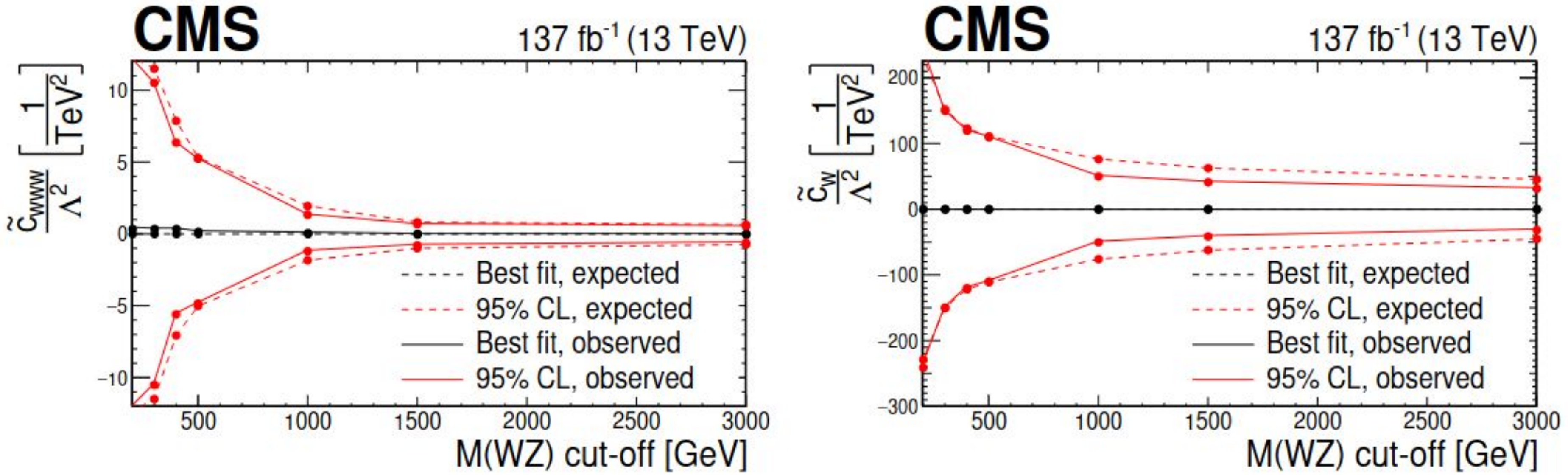

Example 3: ATLAS WZ

WZ rest frame for joint-polarisation and single boson polarisation *(so-called Modified Helicity frame)*

- Allow to meaningfully **compare** both
- **Longitudinal fractions** of both bosons have **maximum decorrelation**

Defined from the joint spin density matrix:

$$\rho_{\lambda_W \lambda'_W \lambda_Z \lambda'_Z} \equiv \frac{1}{C} \times \sum_{\mu_q \mu_{\bar{q}}} F^{(\mu_q \mu_{\bar{q}})}_{\lambda_W \lambda_Z} F^{(\mu_q \mu_{\bar{q}})*}_{\lambda'_W \lambda'_Z} \qquad C = \sum_{\mu_q \mu_{\bar{q}} \lambda_W \lambda_Z} \left| F^{(\mu_q \mu_{\bar{q}})}_{\lambda_W \lambda_Z} \right|^2$$

$$\begin{aligned} f_{00} &= \rho_{0000} \,, \\ f_{TT} &= \rho_{++--} + \rho_{--++} + \rho_{----} + \rho_{++++} \,, \\ f_{0T} &= \rho_{00--} + \rho_{00++} \,, \\ f_{T0} &= \rho_{--00} + \rho_{++00} \,. \end{aligned}$$

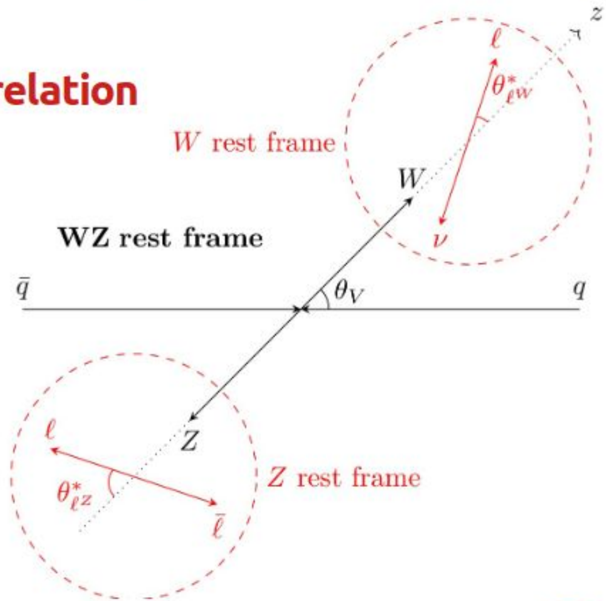

https://indico.cern.ch/event/1252432/contributions/5261540/attachments/2607382/4504015/LHCEWPolarisation-JointPolarisation.pdf

Example 3: ATLAS WZ

Joint-polarisation fraction measurement:

– Analytical variable $|\cos\theta_V|$ not discriminant enough

– **Classification DNN** between all 4 joint-polarisation states: still **poorly discriminant between 0T and T0**

– Split DNN score for 00 in **4 categories** based on cosθ*

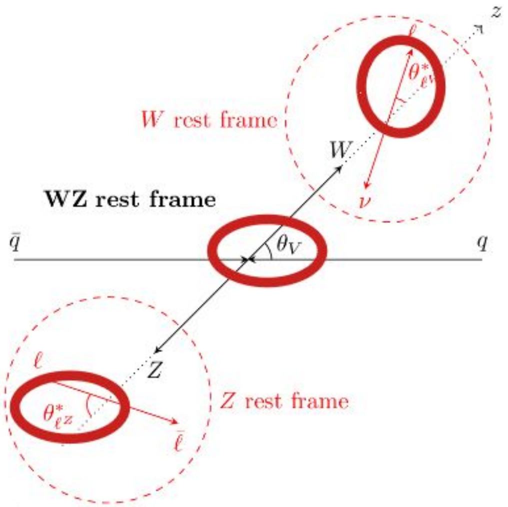

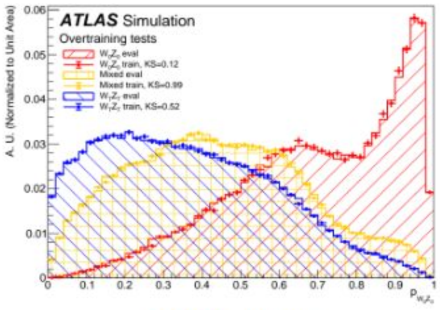

DNN score

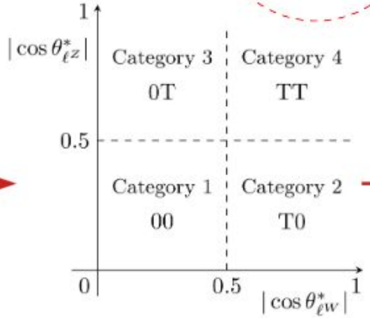

4-categories DNN score

Classification DNN input variables
(by importance)

- $|y_{l,W} - y_Z|$ ~$|\cos\theta_V|$
- P_T^{WZ}
- $P_T^{l,W}$
- $\Delta\varphi(l^W, \nu)$
- $\Delta\varphi(l1^Z, l2^Z)$
- E_T^{miss}
- $P_T^{l2,Z}$
- $P_T^{l1,Z}$

Choice of NLO accurate template set

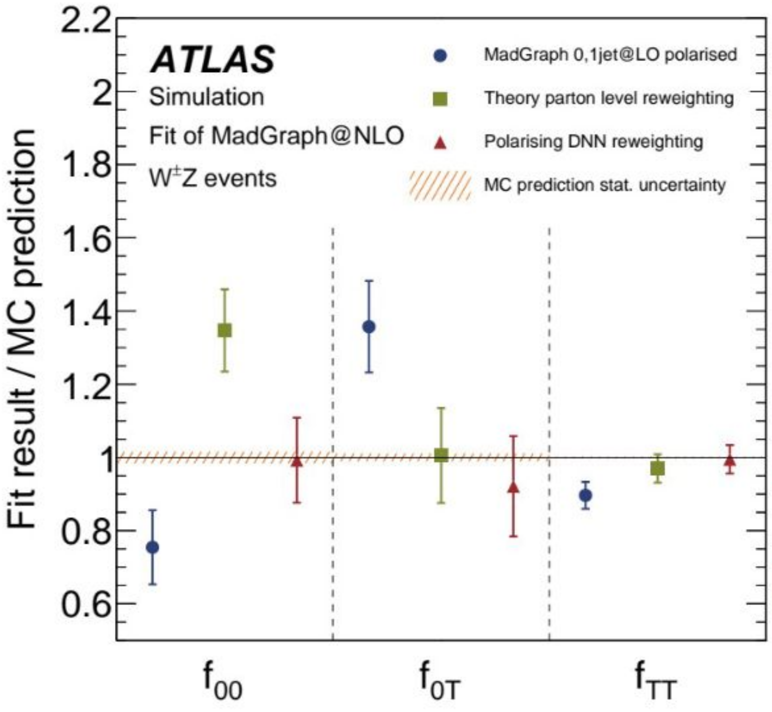

Madgraph polarised generation:

– Big **bias**, from **10% to 40%** of the fractions values

Theory parton level reweighting :

–Still some **bias**, but generally reduced **~15%** of the fractions values

➔ Used as the alternative method for modelling uncertainty

Polarising DNN reweighting :

– Found to be the **least biased method** of all tried (almost no bias)

➔ **Baseline**

arXiv:1907.08209

Example 3: ATLAS WZ

Contents lists available at ScienceDirect

Physics Letters B

journal homepage: www.elsevier.com/locate/physletb

Observation of gauge boson joint-polarisation states in $W^{\pm}Z$ production from pp collisions at $\sqrt{s} = 13$ TeV with the ATLAS detector

The ATLAS Collaboration *

W+ Z & W- Z

f_{00}	0.067 ± 0.010
f_{0T}	0.110 ± 0.029
f_{T0}	0.179 ± 0.023
f_{TT}	0.644 ± 0.032

W+ Z

f_{00}	0.072 ± 0.016
f_{0T}	0.119 ± 0.034
f_{T0}	0.153 ± 0.033
f_{TT}	0.66 ± 0.04

W- Z

f_{00}	0.063 ± 0.016
f_{0T}	0.11 ± 0.04
f_{T0}	0.21 ± 0.04
f_{TT}	0.62 ± 0.05

Measurement performed as well separating by the W charge

- Significance on f_{00} at **6.9σ in W+Z**
- Significance on f_{00} at **4.1σ in W-Z**

Example 4: CMS $W\gamma$

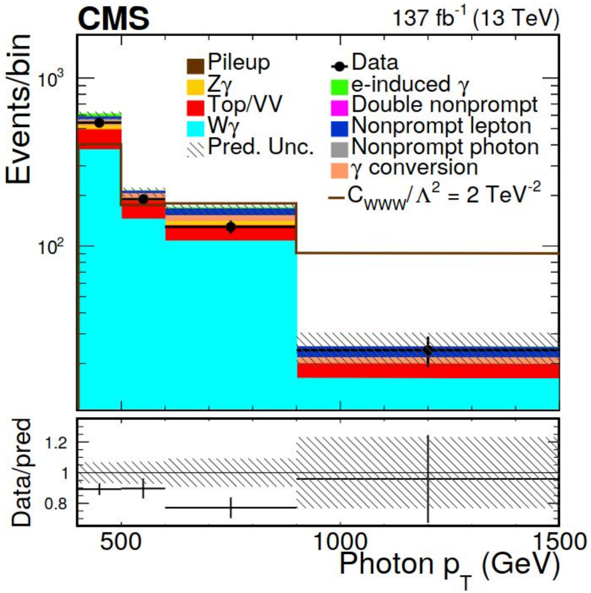

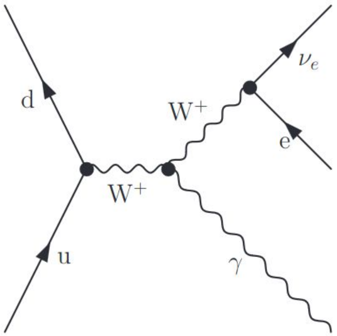

Coefficient	Exp. lower	Exp. upper	Obs. lower	Obs. upper
c_{WWW}/Λ^2	−0.85	0.87	−0.90	0.91
c_B/Λ^2	−46	45	−40	41
$c_{\tilde{W}WW}/\Lambda^2$	−0.43	0.43	−0.45	0.45
$c_{\tilde{W}}/\Lambda^2$	−23	22	−20	20

Figure 3: The photon p_{T} distribution used for the extraction of limits on dimension-six EFT operators. The expected yields correspond to the estimates made before the fit. The uncertainty in the prediction (the hatched band) is the quadratic sum of the systematic uncertainties. The uncertainty in the data is statistical. The last bin includes the overflow.

Summary and Outlook

- **Rich progress and potential from Multiboson Measurements/Probes**
  - Precise measurements, Rare process discovery…
  - Polarization, interference, correlation …
  - Anomalous coupling, EFT, and even Higgs properties…
- **High energy, High Luminosity, High multiplicity, High opportunities!**
- **Rich space for improvement!**
  - CP-odd either ignored, or treated same as CP-even

矢量玻色子散射

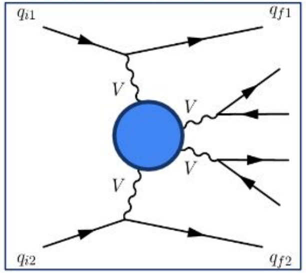

双玻色子产生

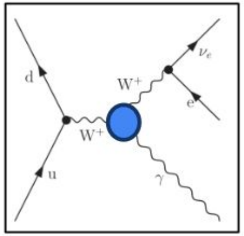

三玻色子产生

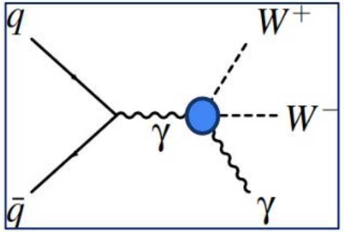

多玻色子共振态

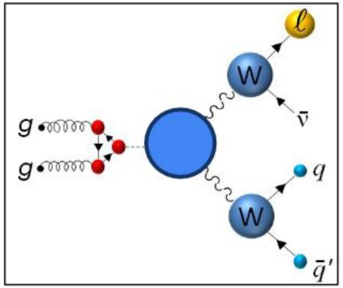

Backup

Higgs without Higgs

TABLE I. Each effect (left-hand column) can be measured as an on-shell Higgs coupling (diagram in the HC column) or in a high-energy process (diagram in the HwH column), where it grows with energy as indicated in the last column.

		HC	HwH	Growth
κ_t	$\mathcal{O}_{y_t}$	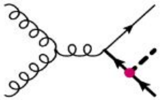	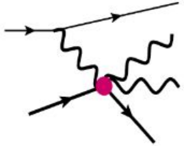	$\sim(E^2/\Lambda^2)$
κ_λ	$\mathcal{O}_6$	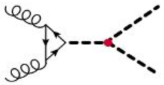	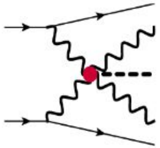	$\sim(vE/\Lambda^2)$
$\kappa_{Z\gamma}$ $\kappa_{\gamma\gamma}$ κ_V	$\mathcal{O}_{WW}$ $\mathcal{O}_{BB}$ $\mathcal{O}_r$	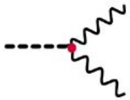	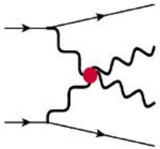	$\sim(E^2/\Lambda^2)$
κ_g	$\mathcal{O}_{gg}$	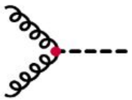	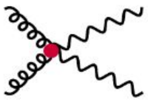	$\sim(E^2/\Lambda^2)$

HCs are associated with an EFT Lagrangian $\mathcal{L} = \sum_i c_i \mathcal{O}_i/\Lambda^2$, consisting in particular of the dimension-six operators [12,13],

$$\mathcal{O}_r = |H|^2 \partial_\mu H^\dagger \partial^\mu H, \qquad \mathcal{O}_{y_\psi} = Y_\psi |H|^2 \psi_L H \psi_R,$$
$$\mathcal{O}_{BB} = g'^2 |H|^2 B_{\mu\nu} B^{\mu\nu}, \qquad \mathcal{O}_{WW} = g^2 |H|^2 W^a_{\mu\nu} W^{a\mu\nu},$$
$$\mathcal{O}_{GG} = g_s^2 |H|^2 G^a_{\mu\nu} G^{a\mu\nu}, \qquad \mathcal{O}_6 = |H|^6, \tag{1}$$

with Y_ψ the Yukawa coupling for the fermion ψ. [Note that the parameters in Eq. (3) can be put in correspondence with other parametrizations of HCs: via partial widths $\kappa_i^2 = \Gamma_{h\to ii}/\Gamma^{\rm SM}_{h\to ii}$ [14], via Lagrangian couplings in the unitary gauge g_{hii} [13,15], or via pseudo-observables [16].]

The operators of Eq. (1) have the form $|H|^2 \times \mathcal{O}^{\rm SM}$, with $\mathcal{O}^{\rm SM}$ a dimension-four SM operator (i.e., kinetic terms, Higgs potential, and Yukawa couplings) times

https://indico.cern.ch/event/1137260/contributions/4779358/attachments/2410006/4123682/LHCEWWG_MB_Presentation(1).pdf

Combinations

$$p_\perp(p_e, p_q) = \vec{p}_e . \left(\vec{p}_{Z/\gamma} \times \vec{p}_q\right)$$

- Different possibilities for the lepton in WZ.
- Explore substitutes of $\vec{p}_{Z/\gamma}$.
- Need to find a substitute to the unobservable $\vec{p}_q$:
  - $\hat{z}$-axis : $[0, 0, 1]$,
  - lepton : $[0, 0, p^z_l]$,
  - neutral boson Z/γ : $[0, 0, p^z_{Z/\gamma}]$,
  - sum of visible particles : $[0, 0, p^z_\sum]$.

Triple products configurations	$\mathcal{O}_{\widetilde{W}WW}$	$\mathcal{O}_{\phi\widetilde{W}B}$
$(\vec{p}_q, \vec{p}_Z, \vec{p}_e)$	-1.612(4)	-0.3888(7)
$(\vec{p}_q, \vec{p}_Z, \vec{p}_{\mu^-})$	-0.184(4)	-0.0271(7)
$\left([0,0,p^z_\sum], \vec{p}_Z, \vec{p}_e\right)$	-0.628(4)	-0.1207(7)
$(\vec{p}_W, \vec{p}_{\mu^-}, \vec{p}_e)$	0.535(4)	0.0965(7)
$(\vec{p}_W, \vec{p}_{\mu^+}, \vec{p}_e)$	0.511(4)	0.1009(7)
$([0,0,p^z_W], \vec{p}_e, \vec{p}_{\mu^-})$	-0.227(4)	-0.0594(7)
$(\vec{p}_W, \vec{p}_{\mu^-}, \vec{p}_{\mu^+})$	-0.080(4)	-0.0110(7)
$\left([0,0,p^z_\sum], \vec{p}_W, \vec{p}_Z\right)$	-0.045(4)	-0.0086(7)
$([0,0,p^z_e], \vec{p}_{\mu^-}, \vec{p}_W)$	0.028(4)	0.0061(7)
$(\vec{p}_e, \vec{p}_{\mu^-}, \vec{p}_{\mu^+})$	-0.025(4)	-0.004(7)
$([0,0,p^z_e], \vec{p}_{\mu^-}, \vec{p}_{\mu^+})$	-0.029(4)	-0.0061(7)
$([0,0,p^z_{\mu^-}], \vec{p}_e, \vec{p}_{\mu^+})$	-0.213(4)	-0.0244(7)
$([0,0,p^z_{\mu^+}], \vec{p}_{\mu^-}, \vec{p}_e)$	0.252(4)	0.0327(7)
$\left([0,0,p^z_\sum], \vec{p}_e + \vec{p}_{\mu^-}, \vec{p}_{\mu^+}\right)$	-0.362(4)	-0.0582(7)
$\left([0,0,p^z_\sum], \vec{p}_e + \vec{p}_{\mu^+}, \vec{p}_{\mu^-}\right)$	-0.300(4)	-0.0481(7)
$\left([0,0,p^z_\sum], \vec{p}_e - \vec{p}_{\mu^-}, \vec{p}_{\mu^+}\right)$	-0.047(4)	-0.0097(7)
$\left([0,0,p^z_\sum], \vec{p}_e - \vec{p}_{\mu^+}, \vec{p}_{\mu^-}\right)$	-0.160(4)	-0.0279(7)

https://indico.cern.ch/event/1137260/contributions/4779358/attachments/2410006/4123682/LHCEWWG_MB_Presentation(1).pdf

Sign of the Interference

- $$\boxed{\mathcal{M}_{int,i} \equiv 2Re\left\{\frac{C_i}{\Lambda^2}\mathcal{M}_i \times \mathcal{M}^*_{SM}\right\}.}$$
  $\mathcal{M}_{int,i}$ is not positive-definite over the phase space but fluctuates.
- Positive and negative contributions perfectly compensates in CP-even observables of a C-even processes. Two suppression mechanisms : Λ^r and sign of $\mathcal{M}_{int}$.
- Ineffectiveness of the cross section and poor constraints on CP-odd operators.

$\Longrightarrow$ Use asymmetries to build CP-odd observables !

https://indico.cern.ch/event/1137260/contributions/4779358/attachments/2410006/4123682/LHCEWWG_MB_Presentation(1).pdf

Asymmetries

- Differential cross section with respect to a CP-odd observable X after a CP-odd $\mathcal{O}_i^6$ insertion is

$$\frac{d\sigma}{dX} = \frac{d\sigma(SM)}{dX} + \frac{C_i}{\Lambda^2}\frac{d\sigma(\mathcal{O}_i)}{dX} + \mathcal{O}\left(\Lambda^{-3}\right).$$

- We define the asymmetry in X as

$$\Delta X = \sigma_{X>0} - \sigma_{X<0} \approx \Delta\sigma_X(SM) + \frac{C_i}{\Lambda^2}\Delta\sigma_X(\mathcal{O}_i),$$

with $\sigma_{X>0} = \int_0^{b_+} \frac{d\sigma}{dX}\, dX$ and $\sigma_{X<0} = \int_{b_-}^{0} \frac{d\sigma}{dX}\, dX$.
$b_\pm$ are the upper and lower bounds of integration of X.

https://indico.cern.ch/event/1137260/contributions/4779358/attachments/2410006/4123682/LHCEWWG_MB_Presentation(1).pdf

Other CP-odd observables in Diboson

"Probing CP-violation at colliders throughinterference effects in diboson production and decay", J. Kumar et al., arXiv 0801.2891

$$\Xi^z_{\pm}(p_Z, p_l) = sign\,(p^z_Z)\,sign\,[(p_l \times p_Z)^z] = sign([0, 0, p^z_Z].\,(\vec{p}_l \times \vec{p}_Z))$$

$$\to \Delta\Xi^z_{\pm} = \Delta p_{\perp}(p_e, p^z_Z)$$

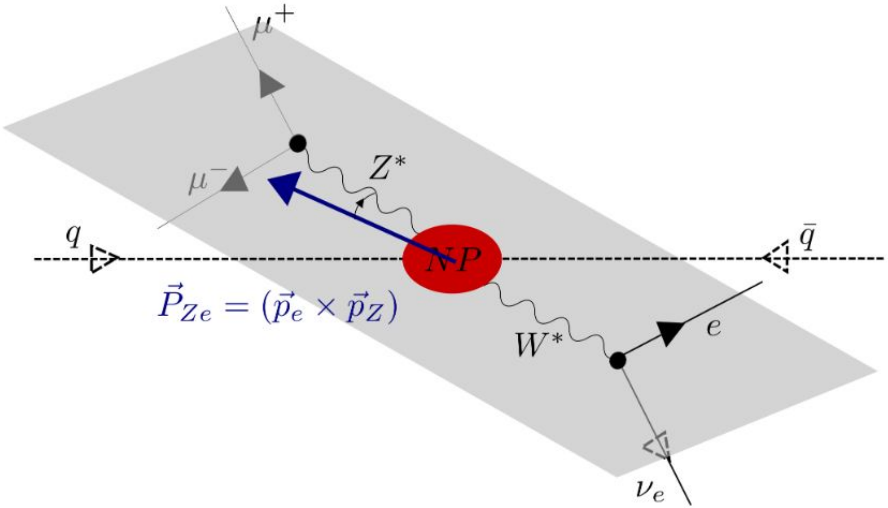

http://cds.cern.ch/record/2865481/files/ATLAS-CONF-2023-038.pdf

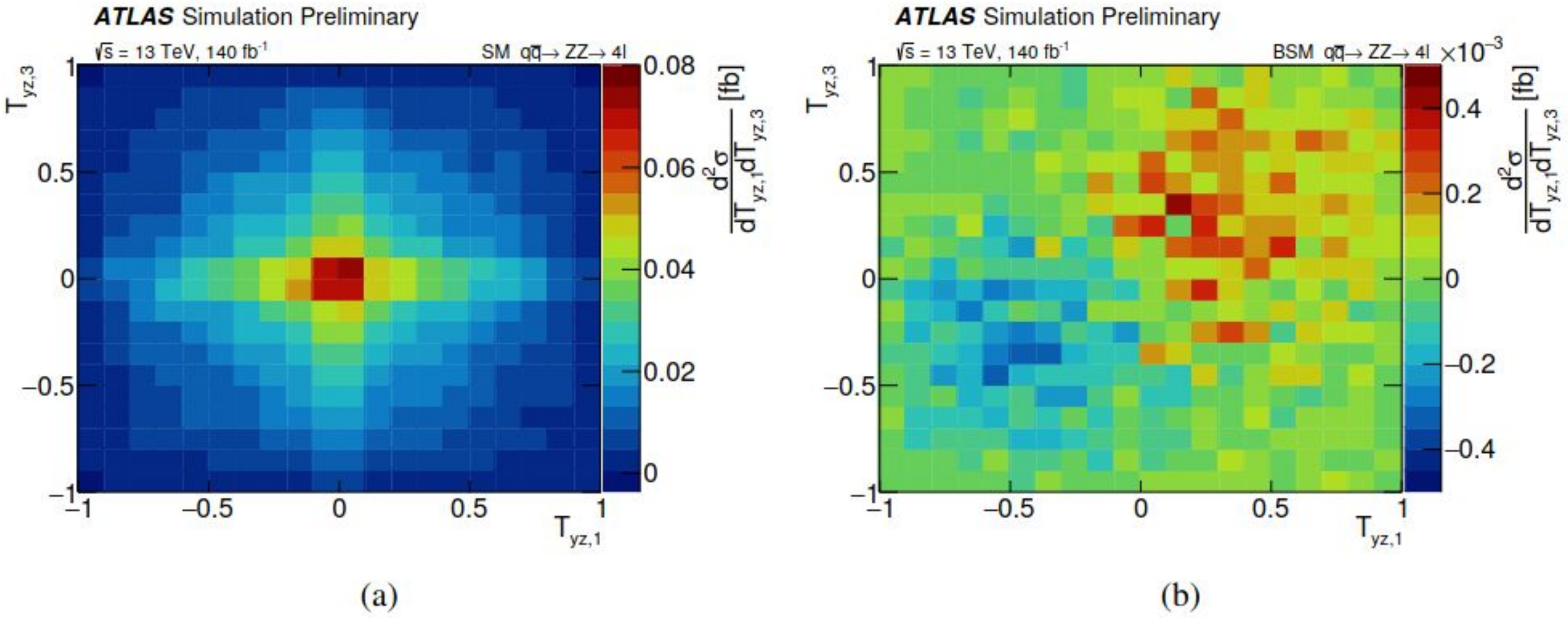

Figure 4: Particle level 2D differential cross-sections of T_{yz} of the two Z bosons for the $q\bar{q} \rightarrow ZZ \rightarrow 4\ell$ process as predicted by (a) the SM and (b) in the presence of the BSM aNTGC vertex. The BSM prediction shows the linear only contribution when $f_Z^4 = 1$.

http://cds.cern.ch/record/2865481/files/ATLAS-CONF-2023-038.pdf

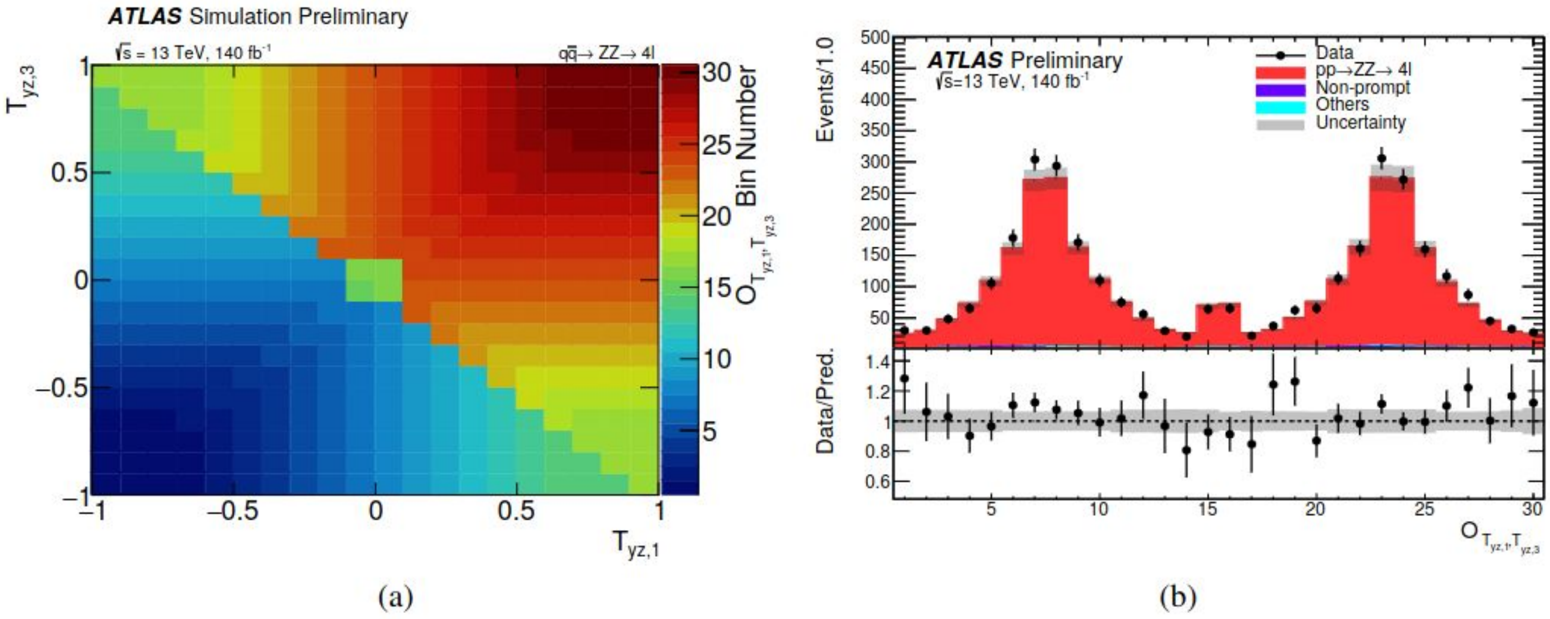

Figure 5: The $2D \rightarrow 1D$ mapping (a) and (b) the detector level measurement of the Optimal Observable $O_{T_{yz,1},T_{yz,3}}$. The measured distribution is compared to the SM signal prediction and the total background. The 'Others' category includes the contribution from $t\bar{t}Z$ and VVZ processes. The non-prompt background is estimated using the fake-factor method. The grey band represents the effect of the total theoretical and experimental uncertainties for the detector-level predictions, and the vertical error bars on data represent the statistical uncertainties.

CMS WZ

The relations described by Eqs. 9 and 10 describe the differential cross sections only when no kinematic requirements are applied to the decay products of the W and Z bosons. Since measured data are limited by the detector acceptance and trigger thresholds, this condition is not fulfilled, thus rendering impossible any direct extraction of the parameters from a fit to a quadratic distribution. Instead, the signal extraction procedure is based on the separation of the WZ process into the three different polarization components (left, right, and longitudinal) based on the generator-level information. The nominal WZ sample is split into three exclusive ones, one for each polarization fraction. Events in the sample are then weighted based on the generator-level $\cos(\theta_{\mathrm{W}})$ ($\cos(\theta_{\mathrm{Z}})$) distributions to match the expected quadratic dependence associated with the corresponding polarization state. The corresponding expected polarization fractions needed to perform this weighting are extracted from an analytical fit of the $\cos(\theta_{\mathrm{W}})$ ($\cos(\theta_{\mathrm{Z}})$) distributions with no kinematic requirements applied, as depicted in Fig. 9. These results for the expected polarization fractions have been cross-checked using an alternative derivation based on the mean and quadratic mean values of the $\cos(\theta_{\mathrm{W}})$ ($\cos(\theta_{\mathrm{Z}})$) quantity in the samples, showing consistent results within the uncertainties presented in the figure. The low p-value for the positively charged $\cos(\theta_{\mathrm{W}})$ fit originates from a fluctuation in the 2016 MC sample. Using these weighted samples, simulation-based templates of the $\cos(\theta_{\mathrm{W}})$ ($\cos(\theta_{\mathrm{Z}})$) distributions at the reconstruction level for each of the polarization states are produced to model each of the polarized final-state contribution.

The polarization measurements are provided separately for the W and Z bosons, following a similar procedure. Since the polarization in the two different charged states can be different,

ATLAS WZ

As observed in theory calculations [23], a strong relationship exists between NLO QCD corrections and polarisation effects. Therefore, templates for helicity states generated at LO are insufficient. The MadGraph 0,1j@LO MC simulation corrects for the real part of NLO QCD effects but misses virtual corrections that are also important for polarisation measurements. In order to verify that the shapes of the polarised templates are valid, a closure test is performed. Templates are used to fit pseudo-data generated using inclusive MC simulations at NLO QCD accuracy, such as with Powheg+Pythia or MadGraph5_aMC@NLO+Pythia. The fit is performed on detector-level distributions. Polarisation fractions extracted from the fit are compared with the generated polarisation fractions of the NLO MC samples. Differences from 10% to 50% depending on the polarisation state are observed between extracted and built-in fractions when using polarised templates from the MadGraph 0,1j@LO generation. This demonstrates the need for using polarised templates at NLO QCD accuracy for polarisation measurements.

Templates better approaching the NLO QCD accuracy are built using a DNN-based event-by-event reweighting procedure [83]. Four DNNs are trained and each of them is specialised to reweight at particle-level the inclusive MadGraph 0,1j@LO events to one of the four joint polarised states. Input variables of the DNNs are those of the polarisation DNN classifier augmented by the invariant mass of the WZ system m_{WZ}, and the angular variables $\cos\theta^*_{\ell W}$, $\cos\theta^*_{\ell Z}$ and $|\cos\theta_V|$. The four DNNs are then applied to reweight the inclusive Powheg+Pythia MC events, creating four polarised MC templates with NLO-like accuracy in QCD. This method provides the best fit closure, with no bias on the extracted polarisation fractions visible within the statistical precision of the closure test.

A second method is used to create NLO QCD accurate polarised templates, based on the available fixed-order parton-level theory predictions [23]. Predicted distributions, including the output score of the DNN classifier, are calculated in the parton-level fiducial phase space [23]. Corrections for parton-shower

ATLAS WZ

Reweighting to theory prediction

In collaboration with theorists **A. Denner, G. Pellicciioli :** Theoretical calculations [arXiv:2010.07149] performed

- in the analysis **fiducial phase** space
- **NLO QCD** polarised → at **parton level**,

➔ Several distributions including the analysis **classification DNN score**

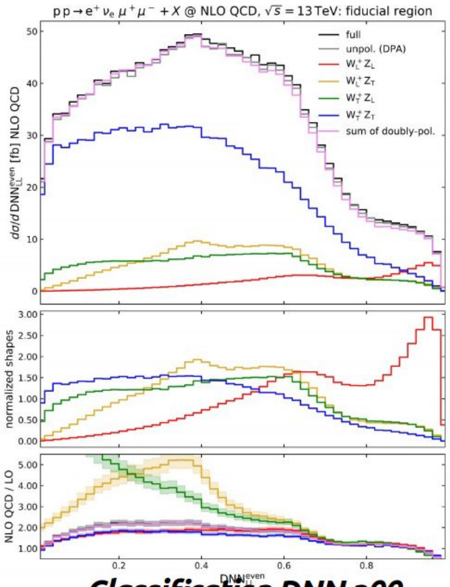

Classification DNN p00 polarised distribution at NLO QCD

[private communication from A. Denner, G. Pellicciioli]

Reweight MG0,1jet polarised to NLO **at parton level** event-by-event with *K*-factor

$$\boxed{K_{\mathrm{MG\,p.s.}} = \frac{\mathrm{MoCaNLO}^{parton}_{\mathrm{pol.}}}{\mathrm{MadGraph}^{parton}_{ref,\mathrm{pol.}}}}$$

13

ATLAS WZ

DNN reweighting

Possible to reweight a distribution using a DNN [arXiv:1907.08209]

➔Acts as a **multi-dimensionnal reweighting** of the input MC sample

4 DNN **trained on polarised Madgraph samples** to discriminate one joint-polarisation states against the inclusive : event-by-event output used in **reweighting**

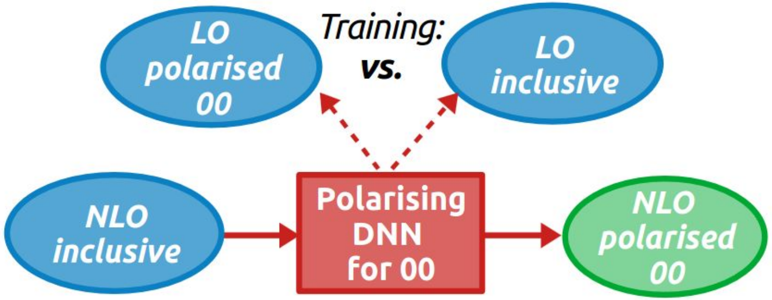

w(x)~ DNN(x) / (1 – DNN(x))

$$|y_{\ell,W} - y_Z|$$
$$p_{\mathrm{T}}^{\ell,W}$$
$$E_{\mathrm{T}}^{\mathrm{miss}}$$
$$\Delta\phi(\ell^W, \ell^\nu)$$
$$p_{\mathrm{T}}^{WZ}$$
$$p_{\mathrm{T}}^{\ell 1,Z}$$
$$p_{\mathrm{T}}^{\ell 2,Z}$$
$$\Delta\phi(\ell 1^Z, \ell 2^Z)$$
$$m_{WZ}$$
$$\cos(\theta^*_{\ell W})$$
$$\cos(\theta^*_{\ell^Z_{ss}})$$
$$\cos(\theta_V)$$

Reweighting DNNs input variables

CMS Wγ

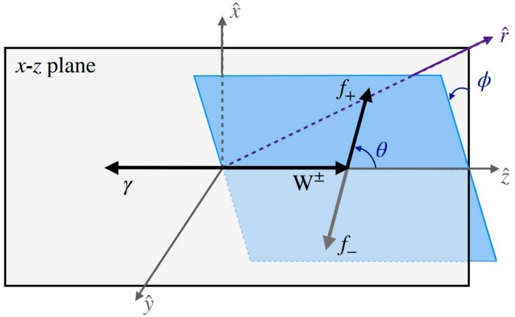

Figure 2: Scheme of the special coordinate system for $W^\pm\gamma$ production, defined by a Lorentz boost to the center-of-mass frame along the direction $\hat{r}$. The z axis is chosen as the $W^\pm$ boson direction in this frame, and y is given by $\hat{z} \times \hat{r}$. The $W^\pm$ boson decay plane is indicated in blue, where the labels f_+ and f_- refer to positive and negative helicity final-state fermions. The angles ϕ and θ are the azimuthal and polar angles of f_+.

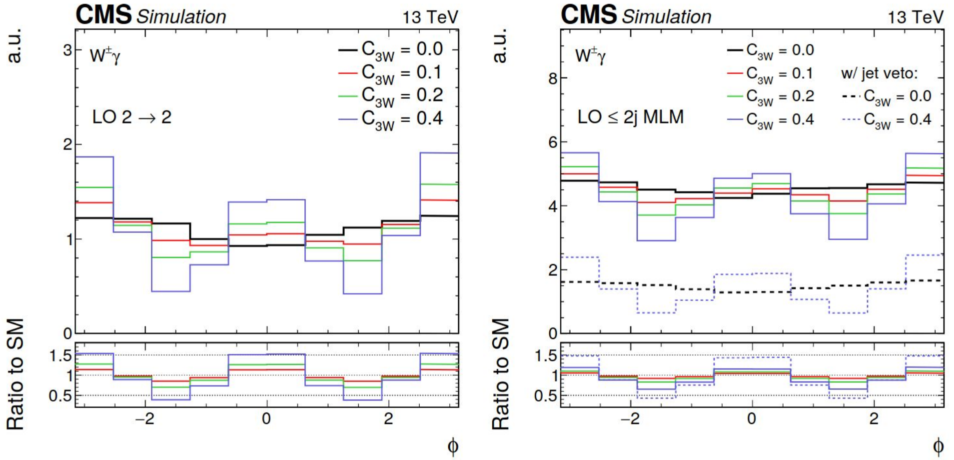

η^ℓ is the pseudorapidity of the lepton, and m_T is the transverse mass of the $\ell\nu$ system. Of the two possible solutions for η^ν, only one will correspond to the unknown true value. One of the two solutions is picked at random event-by-event. In the limit of high $W^\pm$ boson momentum, it can be demonstrated that the two solutions for ϕ, ϕ^+ and ϕ^-, are related by $\phi^+ = \pi - \phi^-$, modulo 2π. This intrinsic ambiguity does not, however, prevent the observation of the interference effect. This is illustrated in Fig. 3, where the deviation in the ϕ distribution is unaffected by a transformation $\phi \to \pi - \phi$.

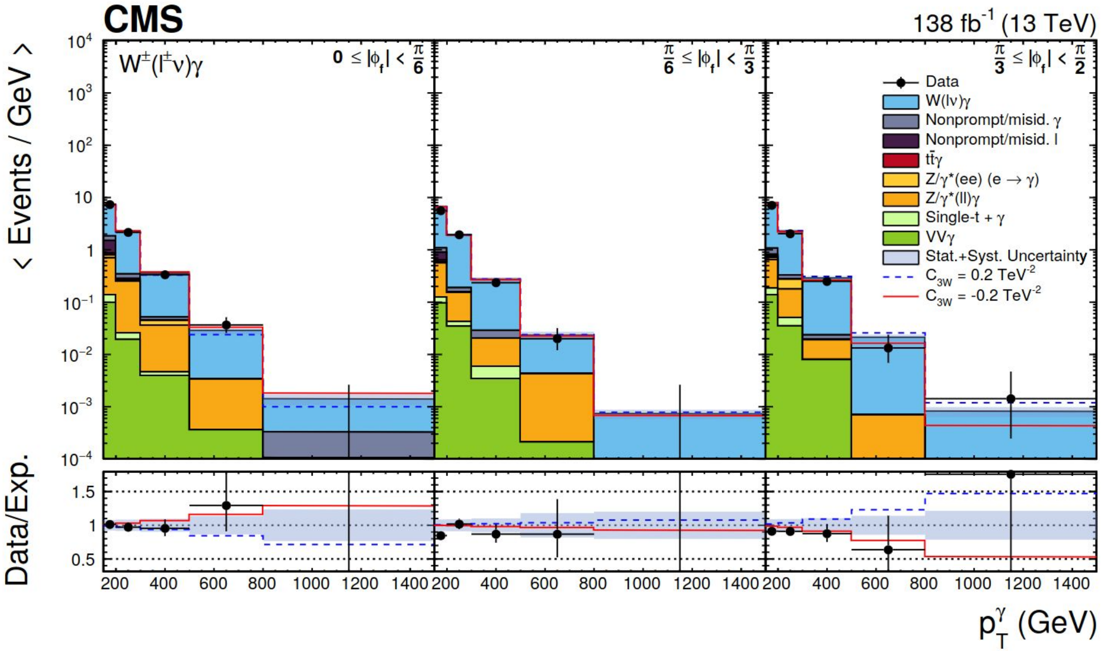

Table 4: Best fit values of C_{3W} and corresponding 95% CL confidence intervals as a function of the maximum p_T^{γ} bin included in the fit.

p_T^{γ} cutoff (GeV)	Best fit C_{3W} (TeV^{-2})		Observed 95% CL (TeV^{-2})		Expected 95% CL (TeV^{-2})	
	SM+int. only	SM+int.+BSM	SM+int. only	SM+int.+BSM	SM+int. only	SM+int.+BSM
200	−0.86	−0.24	[−2.01, 0.38]	[−0.76, 0.40]	[−1.16, 1.27]	[−0.81, 0.71]
300	−0.25	−0.17	[−0.81, 0.34]	[−0.39, 0.28]	[−0.56, 0.60]	[−0.33, 0.33]
500	−0.13	−0.025	[−0.50, 0.25]	[−0.15, 0.12]	[−0.35, 0.38]	[−0.17, 0.16]
800	−0.20	−0.033	[−0.49, 0.11]	[−0.10, 0.08]	[−0.29, 0.31]	[−0.097, 0.095]
1500	−0.13	−0.009	[−0.38, 0.17]	[−0.062, 0.052]	[−0.27, 0.29]	[−0.066, 0.065]